University of Plymouth

PEARL **https://pearl.plymouth.ac.uk**

Faculty of Health: Medicine, Dentistry and Human Sciences Peninsula Medical School

2023-11

Gelation of cytoplasmic expanded CAG RNA repeats suppresses global protein synthesis

Pan, Y

https://pearl.plymouth.ac.uk/handle/10026.1/21551

10.1038/s41589-023-01384-5
Nature Chemical Biology
Springer Science and Business Media LLC

All content in PEARL is protected by copyright law. Author manuscripts are made available in accordance with publisher policies. Please cite only the published version using the details provided on the item record or document. In the absence of an open licence (e.g. Creative Commons), permissions for further reuse of content should be sought from the publisher or author.

The Gelation of Cytoplasmic CAG Repeat Expansion RNAs Suppresses Global Protein Translation

Authors: Yuyin Pan[1$,] Junmei Lu[1$], Xinran Feng[1$], Shengyi Lu[1$], Yi Yang[2], Guang Yang[1], Shudan Tan[1], Liang Wang[3], Pilong Li[3], Shouqing Luo[2*], Boxun Lu[1*].

Affiliations:

[1]Neurology Department at Huashan Hospital, State Key Laboratory of Medical Neurobiology and MOE Frontiers Center for Brain Science, New Cornerstone Science Laboratory, School of Life Sciences, Fudan University, Shanghai, China.

[2]Peninsula Medical School, University of Plymouth, Plymouth, PL6 8BU, UK.

[3]Beijing Advanced Innovation Center for Structural Biology & Frontier Research Center for Biological Structure, School of Life Sciences, Tsinghua University, Beijing, 100084, China

$: these authors contributed equally

*Correspondence to:

Boxun Lu: luboxun@fudan.edu.cn

Shouqing Luo: shouqing.luo@plymouth.ac.uk

Abstract:

RNA molecules with the expanded CAG repeat (eCAGr) may undergo sol-gel phase transitions *in vitro*, but the cellular RNA condensates (foci) are mainly in the nuclei and display liquid-like properties[1]. The functional impact of RNA gelation is also completely unknown. Here, we demonstrate that eCAGr RNA may form cytoplasmic gel-like foci that were rapidly degraded by lysosomes in a LAMP2C-dependent manner. These RNA foci may cause a significant reduction of the global protein synthesis rate in cells and *in vitro*, possibly by sequestering the protein translation elongation factor eEF2. Disrupting the eCAGr RNA gelation restored the global protein synthesis rate, whereas enhanced gelation induced by an optogenetic system exacerbated this phenotype. eEF2 puncta were significantly enhanced in brain slices from a knockin mouse model and patients of Huntington's disease, which is a CAG expansion disorder expressing the eCAGr RNA. Finally, neuronal expression of the eCAGr RNA by AAV injection caused significant behavioral deficits and electrophysiological changes *in vivo* in the mouse model. Our study demonstrates the existence of RNA gelation inside the cells and reveals its functional impact, providing new mechanistic insights into repeat expansion diseases and global protein synthesis regulation.

Main Text:

Nucleotide repeat expansion is the common cause of many inherited diseases[2]. Among them, Huntington's Disease (HD) and certain types of spinocerebellar ataxias are caused by genes containing expanded CAG repeat (eCAGr) sequences[3]. Why these diseases only manifest beyond a threshold number of CAG repeats is a critical question in the field. The prevailing view is that the eCAGr RNA-encoded expanded polyQ stretch beyond the threshold length is the dominant contributor to the disease pathology. Meanwhile, the consecutive CAG-repeat number rather than the polyQ length correlates with the age-of-onset of HD[4], suggesting other possible etiologies underlying the toxicity of the polyQ. Repeat-associated non-ATG (RAN) translation products were detected in several eCAGr diseases[5-7], but their pathogenic contribution remains controversial[8]. The potential loss of wild-type protein function[9-11] and the eCAGr RNA toxicity[12, 13] may also contribute to the disease, but their contribution and mechanism need further confirmation.

The liquid-liquid phase separation (LLPS) and the sol-gel phase transition (PT, or gelation) provide a new angle to understand the non-coding role of the repeat expansion RNAs. For example, they may perturb the dynamics of stress granules and P-bodies by promoting the phase separation of RNA granule proteins[14]. The eCAGr RNA undergoes LLPS and gelation by itself, but the functional impact is completely unknown[1, 15, 16]. In this study, we aimed at identifying the functional role of eCAGr RNA gelation, which may provide a new scenario beyond the current polyQ protein-dominant understanding of the disease and reveal new biology of RNA foci.

It is interesting to note the contrasting properties between the solid-like *in vitro* eCAGr RNA foci and liquid-like nuclear ones in cells[1]. The increased dynamicity of the nuclear eCAGr RNA foci may arise from RNA-protein interactions in the nucleoplasm, which remodels RNA base-pairing[1]. Yet, it is unclear why cytoplasmic eCAGr RNA foci are largely absent[1, 17] and

whether the RNA gelation does occur in cells. It is critical to investigate the possible formation and properties of cytoplasmic eCAGr RNA foci. Considering that the eCAGr RNA may form foci by itself *in vitro*[1], we speculated that cytoplasmic eCAGr RNA foci may have formed but be rapidly cleared by lysosomal degradation, which is capable of degrading macroaggregates in the cells[18]. The nuclear eCAGr RNA foci could be better preserved because of less lysosomal accessibility.

In this study, we tested this hypothesis and observed gel-like eCAGr RNA foci in the cytoplasm, demonstrating RNA gelation in the cells. We further investigated the functional impact of the eCAGr RNA gelation.

Results

Observation of cytoplasmic eCAGr RNA foci

To visualize repeat-containing eCAGr RNA foci in the cells, we tagged the RNA with MS2-hairpin loops and co-expressing it with the yellow fluorescent protein (YFP)-tagged MS2-coat binding protein (MS2CP–YFP), which is the same system utilized in the original report of eCAGr RNA phase separation[1]. Consistent with the previous report[1], we observed mainly nuclear eCAGr (47×CAG) RNA foci with few cytoplasmic foci in HEK293T cells (Fig. 1a). The observed foci were unlikely caused by possible undegraded MS2 hairpins or clustering of MS2CP, because the short CAG repeat (12×CAG) RNA formed essentially no foci (Fig. 1a), consistent with previous studies using the same system[1]. To further exclude this possibility, we performed the RNA fluorescence in situ hybridization (FISH) of the CAGr RNA and observed long CAG repeat-dependent foci, which largely colocalized with MS2CP puncta (Extended Data Fig. 1a, *left* panels). The number and size of eCAGr RNA foci detected by FISH were also highly similar to the ones detected by MS2CP (Extended Data Fig. 1a, *right* panels), confirming that the MS2CP puncta

faithfully represent the eCAGr RNA foci. The RNA FISH also detected the RNA foci using an MS2 probe without the presence of MS2CP (Extended Data Fig. 1b). We also confirmed the presence of eCAGr RNA foci using MS2-independent approaches by transfection of Cy3-labeled RNA (Extended Data Fig. 1c-d). Finally, we further validated the MS2 system by detecting the eCAGr RNA foci by transfecting Cy3-labeled repeat-containing RNA along with MS2CP (Extended Data Fig.1e) and observed strong co-localization between Cy3-labeled 72×CAG RNA and MS2CP puncta.

The low abundance of cytoplasmic eCAGr RNA foci was unlikely due to threshold-insufficient eCAGr RNA levels, as the exogenous over-expression system probably gave rise to an elevated eCAGr RNA concentration in the cytoplasm. Thus, we speculated that the cytoplasmic eCAGr RNA foci may have been formed, but subject to rapid clearance *via* lysosomes, which are involved in degrading cytoplasmic RNAs[19, 20]. To test this hypothesis, we treated the cells with lysosome inhibitors NH_4Cl, chloroquine (CQ), or bafilomycin A1 (BafA), and observed numerous cytoplasmic RNA foci in most of the cells (Fig. 1a-b). The presence and enrichment of cytoplasmic RNA foci could be caused by an enhancement of foci formation or inhibition of foci degradation. Most of these foci colocalized with lysosomes as detected by both the MS2 system (Fig. 1b) and direct Cy3-labeling of the RNA (Extended Fig. 1d), supporting the latter possibility. To further validate this, we performed live-cell imaging and observed the emergence of eCAGr RNA foci after adding the lysosome inhibitor NH_4Cl (Fig. 1c) as well as the disappearance of these foci after washing out NH_4Cl (Fig. 1d), confirming their lysosomal degradation. Finally, using the MS2-independent FISH approach, we further confirmed the presence of cytoplasmic RNA foci in the HD mouse striatal ($STHdh^{Q7/Q111}$) cells expressing endogenous eCAGr RNA upon NH_4Cl treatment[21] (Fig. 1e). In our later experiments, similar observations were made *in vivo* of brain

slice samples from aged HD mice without NH_4Cl treatment (see Fig. 7c-d). Noticeably, the average size and the largest size of the endogenous CAGr RNA foci were significantly larger in the HD cells (Fig. 1e), suggesting the eCAGr RNA condensation rather than stabilization. In fact, the eCAGr RNA (mutant *Htt*) level was similar to the wild-type *Htt* level both in cells and *in vivo* (Extended Data Fig. 1f). Meanwhile, consistent with the degradation of eCAGr RNA foci *via* the lysosome, the NH_4Cl treatment increased the eCAGr RNA (mutant *Htt*) level but not wild-type *HTT* level (Extended Data Fig. 1g).

LAMP2C-dependent lysosomal degradation of cytoplasmic eCAGr RNA foci

The lysosomal degradation of cytoplasmic eCAGr RNA foci could be mediated by macroautophagy, an intracellular pathway that can remove RNA-associated granules[22-24]. If this were the case, we would anticipate observing substantial cytoplasmic eCAGr foci in macroautophagy-deficient cells (Atg9a, Atg14, or FIP200 knockout cells[25]) even without the treatment of lysosome inhibitors. Surprisingly, the cytoplasmic RNA foci were still largely absent in Atg9a, Atg14, or FIP200 homozygous knockout STHdh cells (Fig. 2a-b; see the knockout sequence validation in Supplementary Fig. 1), suggesting that they were cleared by macroautophagy-independent pathways. RNA molecules could also be degraded by lysosomes *via* RNautophagy, a cellular process in which the RNAs are loaded directly to the lysosomes by LAMP2C[20]. Consistent with the involvement of RNautophagy, we knocked down Lamp2c (Fig. 2c) and observed remarkable cytoplasmic eCAGr foci (47×CAG but not 12×CAG) without treatment of lysosome inhibitors (Fig.2d). In contrast, the knockdown of Lamp2a or Lamp2b did not have such effects (Fig. 2d). Remarkably, none of the cytoplasmic eCAGr foci colocalized with lysosomes in the Lamp2c knock-down cells (Fig. 2d), suggesting that they were not loaded to the lysosomes in the conditions. Taken together, the cytoplasmic eCAGr RNA can form foci, which

are rapidly degraded by lysosomes likely *via* Lamp2c-dependent RNautophagy. This observation is also consistent with previous studies showing that CAG repeat RNA is degraded by RNautophagy *via* SIDT2 and LAMP2C[26].

Cytoplasmic eCAGr RNA foci are degraded rather than induced by lysosome inhibition

The existence of relatively transient cytoplasmic eCAGr RNA foci needs further validation to disprove a scenario in which the lysosomal inhibition leads to increased eCAGr RNA concentrations beyond the sol-gel threshold and induces gelation. The latter scenario is unlikely because the cytoplasmic foci appeared relatively rapidly after lysosome inhibition (Fig. 1c, ~2 hours after NH_4Cl treatment). In addition, the strong colocalization between cytoplasmic RNA foci and the lysosomes (Fig. 1b & Extended Data Fig. 1d) suggests that either the foci were formed and then engulfed by the lysosomes or the lysosomes functioned as docking sites to induce RNA foci formation. The latter possibility is inconsistent with the observation that RNA foci formed outside the lysosomes in cells with *Lamp2c* knocked down (Fig. 2d).

To further demonstrate the engulfment of eCAGr RNA foci into the lysosomes, we performed confocal microscopy to visualize the high-resolution spatial relationship between the eCAGr RNA foci and the lysosomes. The RNA foci could be wrapped but detached from the lysosomal membrane detected by its marker LAMP1 (Extended Data Fig. 1h-i), suggesting that they were engulfed cargoes rather than assembly cores supporting lysosome membranes.

Cytoplasmic eCAGr RNA foci formation without lysosomal inhibition

To further validate the existence of cytoplasmic RNA foci in absence of lysosome inhibition, we performed time-lapse experiments in cells starting to express eCAGr RNA to capture the time window of cytoplasmic RNA foci formation in absence of lysosome inhibitors. Upon induction of the RNA expression in the HEK293T cells, cytoplasmic eCAGr RNA

(47×CAG) foci started to appear after 30 minutes and increased in the first 2 hours (Extended Data Fig. 1j). No such foci were observed in the 12×CAG expressing cells (Extended Data Fig. 1j). Interestingly, without the lysosome inhibitor treatment, almost none of the cytoplasmic eCAGr RNA (green) colocalized with the lysosomes (red) (Extended Data Fig. 1j), likely due to their rapid clearance after their engulfment by the lysosomes. Consistent with this, we tracked the cytoplasmic eCAGr RNA foci in some of the cells and observed their rapid disappearance after their colocalization with the lysosome using both MS2-dependent (Extended Video 1) and MS2-independent approaches (Extended Video 2), validating the conclusion that cytoplasmic foci are formed and then rapidly degraded by lysosomes. Finally, eCAGr RNA with a larger repeat number (72×CAG) could form a few but evident cytoplasmic foci in absence of lysosomal inhibitors (Fig.2e-f), further confirming that cytoplasmic eCAGr RNA foci do exist without lysosomal inhibition.

Cytoplasmic eCAGr RNA foci are solid-like

We then investigated the physical properties of cytoplasmic versus nuclear RNA condensates using the fluorescence recovery after photobleaching (FRAP) approach. The nuclear condensates exhibited liquid-like properties as suggested by the near-complete recovery (Extended Data Fig. 1k). In contrast, cytoplasmic RNA foci exhibited solid-like properties with essentially no recovery in the FRAP experiments using both MS2-dependent and MS2-independent approaches and in cells with LAMP2C knocked down (Fig. 2g & Extended Data Fig.1l), which were similar to those of *in vitro* eCAGr RNA condensates[1]. While the experimental system is the same as the one used in the previous RNA gelation study[1], it is possible that the dynamics of MS2CP is different from the targeting RNA[27]. We confirmed the gelation of cytoplasmic eCAGr RNA by transfecting Cy3-labeled eCAGr RNA directly (Fig. 2g). Thus, the previously described

RNA gelation observed *in vitro* actually occurred in the cytoplasm rather than in the nuclei. These cellular RNA "gels" were not observed previously possibly because they were rapidly degraded by lysosomes.

The eCAGr RNA suppresses global protein synthesis

We then investigated the potential functional impact of these cytoplasmic eCAGr RNA gels. Changes in global protein synthesis rates have been recently reported in models of CAG repeat expansion disorders but remained controversial, with both upregulation and downregulation of global translation rates reported in different studies[28-33]. All these studies proposed that the mutant protein with expanded polyQ is the major cause of the global protein synthesis change, while the potential role of eCAGr RNA foci in the context cannot be excluded in these studies. The *in vitro* translation experiments actually showed that the addition of either the mutant protein with expanded polyQ or the wild-type protein with short polyQ reduced the translation rate to a similar degree[33], and the reduction might have been caused by the buffer of the purchased recombinant purified HTT proteins used in those experiments because the buffer contained CHAPS, which is known to inhibit eIF4E translational activity[34]. Thus, we investigated whether the eCAGr RNA may contribute to the changes in global translation rates.

We observed no significant changes in the viability of HEK293T and STHdh cells expressing exogenous CAGr RNAs (Extended Data Fig. 2a). Meanwhile, expression of the eCAGr RNA (72×CAG) led to an obvious decrease in the global protein synthesis rate, which was measured by the electrophoresis of nascent proteins at various time points using the Click-chemistry based metabolic labeling technique (Fig. 3a). Remarkably, the eCAGr RNA expression for just 24 hours was sufficient to reduce global protein synthesis in HEK293T cells (Fig. 3b, *left*), suggesting that the effects are relatively rapid. We further confirmed this phenomenon in HD cells

expressing endogenous eCAGr RNA, the STHdh$^{Q7/Q111}$ cells[21] (Fig. 3b, *right*). For quantifications see Extended Data Fig. 2b. Noticeably, over-expression of the mutant *HTT* mRNA reduced global protein synthesis in the wild-type cells (STHdh$^{Q7/Q7}$) whereas knock-down of the *HTT* mRNA (Extended Data Fig. 2c) in the HD cells (STHdh$^{Q7/Q111}$) rescued this phenotype (Fig. 3c & Extended Data Fig. 2d), suggesting that the phenomenon was caused by the eCAGr RNA or its products. Finally, to validate this effect at the single-cell level, we performed high-content imaging analysis by a visualized global protein synthesis assay and measured the protein synthesis of hundreds of cells in each group, confirming the role of eCAGr RNA in the suppression of global protein synthesis (Fig. 3d-e). We further confirmed this effect in cells treated with the lysosome inhibitor NH_4Cl or transfected with the *Lamp2c* siRNA (Extended Data Fig. 2e), which enabled significant cytoplasmic eCAGr RNA detection (Fig. 1 & Fig. 2d).

We further confirmed the effect using a reporter system. We transfected the cells with mRNAs encoding the renilla luciferase reporter protein and measured the protein synthesis rates by the luciferase signal (Fig. 3f). Consistent with the global protein synthesis assays, the translation of luciferase reporter protein was significantly reduced in cells expressing endogenous eCAGr RNAs (Fig. 3f). To exclude possible secondary effects in the cells, we tested the effect in an *in vitro* protein translation system using the rabbit reticulocyte lysate. Pre-treatment of eCAGr RNA (72×CAG, at 50 nM) but not the short CAGr RNA (25×CAG) for 5 minutes significantly reduced the translation of the luciferase reporter protein by the *in vitro* protein translation system (Fig. 3g), confirming the eCAGr RNA-mediated translation deficiency. The effects are likely mediated by the eCAGr RNA rather than its protein products because the eCAGr repeat (72×CAG) was preceded by 6-stop codons, likely resulting in negligible protein products, if any [1] (also see Extended Data Fig. 2f-g). In addition, the RNA with the CAA·CAG mixture sequence

(CAA·CAGm) that encodes the same amino acid sequence (72Q) did not suppress protein synthesis (Fig. 3e & g). To further exclude the possibility of the involvement of the protein products from the repeat-associated non-ATG (RAN) translation, we expressed the RAN translation protein products in the cells (Extended Data Fig. 2f-g) and observed no significant decrease in global protein synthesis (Extended Data Fig. 2h).

The RNA gelation is probably the major cause

While encoding the same amino acid sequence as the 72×CAG, the CAA·CAGm RNA did not suppress protein synthesis (Fig. 3e & g), possibly because the CAA·CAG mixture sequence disrupts RNA gelation[1, 35] (also see Extended Data Fig. 1c). Thus, the RNA gelation might be the fundamental cause of reduced global protein synthesis. To test this hypothesis, we disrupted the eCAGr RNA gelation by its binding to oligonucleotide 8×CTG[1] or binding peptide BIND[36] without influencing the protein level (Extended Data Fig. 3a-b). Transfection of 8×CTG or expression of BIND increased the global protein synthesis phenotype in the HD cells but not in the WT cells (Fig. 4a), suggesting that eCAGr RNA gelation is required for the reduction of protein synthesis rates. This was further confirmed in the HEK293T cells expressing 47×CAG RNA versus the controls (Fig. 4b). Quantification of protein synthesis of different molecular weight in HD cells transfected with BIND was shown in Supplementary Fig.2. Meanwhile, it is worth noticing that 8×CTG reduced the *HTT* mRNA level whereas BIND did not (Extended Data Fig. 3c). Thus, the effects of 8×CTG may also partially due to the lowering of the *HTT* mRNA whereas the effects of BIND are most likely mediated by disrupting RNA gelation. To further exclude possible secondary effects in the cells, we performed *in vitro* translation experiments and confirmed that the protein synthesis deficiency caused by eCAGr RNA could be rescued by the addition of BIND (Fig. 4c), probably through disruption of RNA gelation. Although 8×CTG and

BIND were previously published as tools to disrupt RNA foci, they have limitations because of their binding with the eCAGr RNA, which may influence its various functions. Meanwhile, the RNA gelation disruption tools are currently limited. The available small molecule tool, ammonium acetate at 100 mM[1], precipitates total RNA and suppressed global protein synthesis in wild-type cells (not shown). Thus, we cannot completely rule out other possible mechanisms mediating the suppression of global protein synthesis by eCAGr RNA. Meanwhile, RNA gelation is most likely involved. First, BIND and 8×CTG did not influence global translation in wild-type cells expressing no eCAGr RNA, excluding eCAGr RNA irrelevant effects of these tools *per se*. Second, the CAA·CAG RNA or short CAG repeat RNA did not suppress protein synthesis, suggesting that the ability of gelation correlates with the ability to suppress global translation. Third, while BIND and 8×CTG may also influence the protein products including the RAN translation products of eCAGr RNA, these proteins may not influence global protein synthesis even when they were over-expressed (Extended Data Fig. 2f-h). Finally, we later revealed the eCAGr RNA gelation may sequester the key translation factor eEF2 (see Fig. 7 & Extended Data Fig. 7a), suggesting that the gelation is involved in the global protein synthesis suppression.

To further investigate the potential involvement of RNA gelation, we established an optogenetic system that allows us to induce RNA gelation by blue-light exposure (Fig. 4d), based on previous systems designed for protein LLPS and PT[37]. By conjugating the eCAGr RNA-binding peptide BIND to a blue-light sensitive protein Cry2, we managed to control eCAGr RNA gelation (Fig. 4e & Extended Data Fig. 3d) by blue light *via* BIND-Cry2 -eCAGr RNA interaction without causing cytotoxicity (Extended Data Fig. 3e). The blue-light-induced eCAGr RNA foci became solid-like gels in the cytoplasm (Extended Data Fig. 3f), leading to a reduced global translation rate compared to that in the no-light condition (Fig. 4f), under which the foci were disrupted.

Quantifications of replicated experiments in Fig. 4 are shown in Extended Fig. 3g-i. The translation suppression was unlikely resulted from possible stress or toxicity of the blue-light induced clustering of the RNA binding proteins *per se*, because such effects were absent in wild-type cells without eCAGr RNA expression (Fig. 4f & Extended Data Fig. 3i). In addition, while the prolonged blue-light induction may cause cytotoxicity, induction within 15 hours does not lead to detectable cell viability changes based on previous reports[38], consistent with our observation (Extended Data Fig. 3e).

We further utilized this system to distinguish the contribution from cytoplasmic versus nuclear eCAGr RNA foci. We transfected the cells with BIND-Cry2 specifically localized in cytoplasm versus the nucleus (Extended Data Fig. 3j). This was achieved by adding the nuclear export sequence (NES) versus the nuclear localization sequence (NLS) to BIND. Without the blue-light exposure, the NES-BIND-Cry2 but not the NLS-BIND-Cry2 partially rescued the global protein synthesis deficits in the HD cells (Extended Data Fig. 3j), possibly because NES-BIND partially disrupt cytoplasmic eCAGr foci without blue light. In contrast, after exposure to the blue-light, the global translation was suppressed by the NES-BIND-Cry2 but not the NLS-BIND-Cry2 in HD cells (Extended Data Fig. 3j), possibly due to the induction of cytoplasmic eCAGr RNA foci by NES-BIND under the blue-light. The data suggest that the cytoplasmic rather than nuclear eCAGr RNA foci formation is the major contributor to the global translation suppression.

Taken together, we revealed the function of eCAGr RNA gelation in suppressing global protein synthesis.

The eCAGr RNA regulates translation elongation

We then investigated the possible mechanism of eCAGr RNA-induced global protein synthesis suppression. We performed the polysome profiling experiments to investigate the

distribution of mRNAs with different numbers of ribosomes and observed only very subtle differences between HD and WT cells or between cells expressing eCAGr RNA versus the controls (Extended Data Fig. 4a). This suggests that the translation defects were not caused by ribosome assembly deficits[39]. We further confirmed this by electrophoresis of total and cytoplasmic RNA, the qPCR detection of ribosome RNAs (rRNAs) (45S, 28S, and 18S), the electron microscopy of ribosome density, and the nascent rRNA synthesis detected by EU incorporation. We observed no significant differences between HD and WT cells in these experiments (Extended Data Fig. 4b-e). Thus, rRNA expression or assembly changes were unlikely to be the major cause of eCAGr RNA-induced global protein synthesis suppression.

To further analyze potential defects in translation machinery, we performed the SUnSET assay, which detects the total number of translating peptides at a specific time point by the C-terminus puromycin signals[40] (Fig. 5a). The puromycin signals were not decreased in the HD cells (Fig. 5a), suggesting that the number of translating peptides was not decreased in HD cells. Meanwhile, the protein translation elongation impairment may not reduce the number of translating peptides but increase their maturation time instead (Fig. 5b). Consistent with this, knock-down of eEF2, a key translation elongation factor, also failed to decrease the SUnSET signals[41]. This may explain why the SUnSET signals were not decreased while the global protein synthesis was suppressed. Thus, the SUnSET data suggest that the eCAGr RNA may impair the global protein translation elongation rather than initiation.

The experiments above suggest potential defects in protein translation elongation. We further tested this directly using previously established methods. We confirmed the suppression of protein translation elongation in HD cells by the SunRiSE (SUnSET-based Ribosome Speed of Elongation) assay, which measures the maturation of translating peptides when the translation

initiation is blocked[42]. Compared to the control cells, the HD cells exhibited a significantly slower decay of the SunRiSE signals, suggesting an impairment of protein translation elongation in these cells (Fig. 5c). Finally, we characterized the translation elongation directly by the polysome run-off assay, which measures the polysome loss caused by translation elongation when the initiation is blocked[43]. The polysome run-off was significantly reduced in the WT cells expressing 72×CAG RNA or in the HD cells compared to the controls (Fig. 5d), confirming the translation elongation impairment induced by eCAGr RNA.

The eCAGr RNA foci induce the eEF2 clustering and degradation

Elongation factors such as eEF1 and eEF2 play a key role in protein translation elongation[44]. Indeed, the level of total eEF2 was decreased in the HD cells or cells expressing exogenous eCAGr RNA compared to the controls, whereas the level of eEF1A, the central functional component of the eEF1 complex, was not (Fig. 6a). The eEF2 lowering is probably due to its lysosomal clearance because the effect could be blocked by the lysosome inhibitor CQ (Fig. 6a).

With the eEF2 level lowered by eCAGr RNA, we further investigated if eCAGr RNA could compromise eEF2 activity. Phosphorylation of eEF2 is known to interfere with its interaction with ribosomes, leading to reduced eEF2 translational functions[45]. Meanwhile, the level of phosphorylated eEF2 was reduced rather than increased in the HD cells or cells expressing exogenous eCAGr RNA (Fig. 6a), suggesting that eEF2 was not inactivated by eCAGr RNA through eEF2 phosphorylation. The eEF2 lowering was rescued by transfection of 8×CTG (Extended Data Fig. 5a), suggesting that the effect is likely due to eCAGr RNA gelation. eEF2 clustering is also known to suppress its function[46], and thus we visualized eEF2 in the cells by immunofluorescence or fluorescent protein tagging. In the absence of lysosome inhibition, the

basal diffused eEF2 level was lower in the HD (STHdh$^{Q7/Q111}$) cells than in the WT (STHdh$^{Q7/Q7}$) cells (Extended Data Fig. 5b), consistent with the western-blots (Fig. 6a). After treatment of the lysosome inhibitor NH_4Cl, the HD cell exhibited significantly more eEF2 puncta than the wild-type cells (Extended Data Fig. 5b). Cytoplasmic eEF2 puncta were also significantly increased in brain slices from aged human HD patients (Fig. 6b) or HD mice (Hdh$^{Q7/Q140}$) (Fig. 6c & Extended Data Fig. 5c), suggesting that eEF2 clustering could be a mechanism *via* which the eCAGr RNA influences global translation elongation.

The eEF2 puncta in eCAGr RNA-expressing cells are likely to be solid-like condensates because they failed to recover after photo-bleaching (Extended Data Fig. 5d). The cells were treated with the lysosome inhibitor NH_4Cl to avoid the potential lysosomal clearance of the eEF2 puncta so that they could be visible. These eEF2 puncta and eCAGr RNA foci colocalized with the lysosomes, confirming their lysosomal degradation (Extended Data Fig. 5e-f).

To confirm that the eEF2 clustering was caused by eCAGr RNA gelation, we utilized the optogenetic system to induce the enhanced eCAGr RNA clustering and tracked eEF2 in live cells. Blue-light exposure led to drastic eEF2 puncta formation (Fig. 6d), confirming eEF2 clustering as a consequence of eCAGr RNA gelation.

To further elucidate the functional relevance of eEF2 changes in HD cells or cells expressing exogenous eCAGr RNA, we investigated eEF2's distribution in different fractions of the polysome profiling samples and observed a significant reduction of eEF2 in the ribosomal subunit and monosome fractions of HD cells with or without lysosome inhibition (Extended Data Fig. 6a), suggesting that eEF2 dissociated with ribosomes in eCAGr RNA-expressing cells. The dissociation of eEF2 from the ribosomes could be rescued by disrupting the eCAGr RNA foci with 8×CTG (Extended Data Fig. 6a), confirming the role of the eCAGr RNA. Consistent with this, the

colocalization between eEF2 and the ribosomal marker Rps6 was significantly reduced in the HD cells compared to the WT, whereas the eEF1A-Rps6 colocalization remained the same (Extended Data Fig. 6b). In the *in vitro* translation system, the addition of the recombinant eEF2 protein (Supplementary Fig. 3) rescued the translation deficits in the eCAGr RNA treated group (Fig. 6e). Taken together, loss-of-function of eEF2 by its clustering and lysosomal clearance may mediate the eCAGr RNA-induced suppression of global protein synthesis.

eCAGr RNA foci sequester eEF2

Why eCAGr RNA gelation may cause eEF2 clustering is intriguing. Our *in vitro* experiments showed that the recombinant eEF2 protein (Supplementary Fig. 3) at relatively physiological conditions (62.5 to 500 nM) was able to form condensates in saline only with the presence of eCAGr RNA but not short CAG repeat RNA (Extended Data Fig. 7a), suggesting that the formation of eEF2 condensates could be facilitated by the eCAGr RNAs. We also observed strong colocalization between eEF2 and eCAGr RNA condensates (Extended Data Fig. 7a). In contrast, GFP failed to form condensates with eCAGr RNA (Extended Data Fig. 7a). eEF1a formed condensates but had a weaker colocalization with eCAGr RNA foci compared to eEF2 condensates, at least at low concentrations (Extended Data Fig. 7a). The interaction between eCAGr RNA and eEF2 could be detected by biochemical approaches including Electrophoretic Mobility Shift Assay (EMSA) and RNA-immunoprecipitation (RNA-IP) experiments (Extended Data Fig. 7b-c). Taken together, the *in vitro* experiments demonstrate a possibility that eCAGr RNA gels sequester and co-cluster with eEF2 to form condensates, although the *in vitro* conditions could be different from those in the cells.

We then investigated this possibility by visualizing the colocalization between the eEF2 puncta and the eCAGr RNA foci in cells treated with the lysosome inhibitor NH_4Cl. In WT cells

(STHdh$^{Q7/Q7}$) co-expressing the eCAGr RNA (47×CAG-MS2) and GFP-fused eEF2, we observed strong colocalization between these two, with the RNA being detected by MS2CP-BFP (Fig. 7a). Such colocalization was not observed in the control groups expressing 12×CAG-MS2 with eEF2 or 47×CAG-MS2 with eEF1A (Fig. 7a), confirming that the colocalization is unlikely due to possible artifacts from the MS2 system. Such colocalization was also observed between GFP-fused eEF2 and endogenous eCAGr RNA foci in HD (STHdh$^{Q7/Q111}$) but not WT (STHdh$^{Q7/Q7}$) cells (Extended Data Fig.7d) using the MS2-independent FISH approach. Finally, in cells without the treatment of NH_4Cl but with *Lamp2c* knocked-down, we also observed a similar colocation between eCAGr RNA (47×CAG-MS2) and endogenous eEF2(Fig.7b). To further demonstrate such colocalization in an *in vivo* system at the endogenous level, we visualized the foci of endogenous mutant *HTT* mRNA harboring eCAGr and endogenous eEF2 protein in the same cortical and striatal brain slices from an HD knock-in model Hdh$^{Q7/Q140}$ using RNA FISH and immunofluorescence, respectively (Fig. 7c-d; the eEF2 antibody specificity was validated in Extended Data Fig. 7e). Noticeably, the observed eCAGr RNA foci in the brain slices are likely due to RNA gelation rather than RNA stabilization, because their foci number and size were significantly larger in the HD samples than the ones observed in the wild-type (Fig. 7c-d), whereas the *HTT* RNA level was similar or even lower than the one in the wild-type (Extended Data Fig. 1g). The presence of many colocalized eEF2 puncta and eCAGr RNA foci suggests defects in their lysosomal clearance in these animals. Consistent with this, the key lysosome proteases CSTB and CSTD have reduced activity in HD brains (Extended Data Fig. 8a). Meanwhile, the *Lamp2c* mRNA expression was not significantly reduced in the HD brains (Extended Data Fig. 8b). This may explain the strong colocalization between eEF2 and the lysosome marker Lamp1 in the mouse

brain (Extended Data Fig. 8c), illustrating that eEF2 puncta may enter the lysosomes but not be degraded efficiently by the lysosomes in the HD brains.

Taken together, cytoplasmic eCAGr RNA may form solid-like foci similarly to its behaviour *in vitro*[1] (Fig. 2g), and these foci may sequester eEF2, leading to loss of eEF2 function in translation elongation (Fig. 7e).

Potential contributions to pathophysiology

We then investigated whether eCAGr RNA may contribute to disease pathophysiology *in vivo* in the mouse model. Mouse models of CAG repeat expansion disorder such as Huntington's disease usually exhibit almost no neuronal loss[47, 48], and thus we focused on possible behavioral and physiological deficits. We injected the wild-type mouse striatum with AAV expressing different RNAs (25×CAG, 72×CAG, CAA·CAGm, and ATG-CAA·CAGm) in the neurons driven by the human SYN1 promoter (Fig. 8a-b). At the 5' end, the first three RNAs have 6 stop-codons whereas the ATG-CAA·CAGm RNA has the ATG start codon. The 25×CAG and CAA·CAGm groups expressing CAG-containing RNAs with little gelation were used as negative controls. The ATG-CAA·CAGm RNA leads to the expression of the polyQ protein, which is a positive control and the known major contributor to polyQ diseases[49]. The 72×CAG group is the test group expressing eCAGr RNA with significant gelation. Different RNAs were expressed at a similar level (Fig. 8c). 4 weeks after AAV injection, we performed several typical motor-function-related behavioral and neuro-transmission-related electrophysiological tests widely used for polyQ disease studies. We observed significant behavioral deficits of the 72×CAG group in the balance beam and rotarod tests (Fig. 8d-e). We also observed a similar trend in the rearing/climbing test, although not in the gripping force test (Extended Data Fig. 9a-b). The data suggest possible functional deficits in neurons. Consistent with this, electrophysiological recording of the striatal

slices revealed a significantly decreased amplitude of outward K^+ currents in the 72×CAG RNA-expressing neurons (Fig. 8f), consistent with the observation in striatal neurons from HD mice[50]. The spontaneous excitatory postsynaptic current (sEPSC) was also changed by 72×CAG RNA expression, exhibiting significantly reduced sEPSC frequency (Fig. 8g-h). The event distribution of sEPSC frequency, amplitude, and interval time was also shifted in the direction of reduced synaptic strength (Fig. 8h-j), consistent with the observation in the HD mice[51] and the effects of protein synthesis suppression[52], suggesting potential pathophysiological impacts of the eCAGr RNA-induced suppression of global protein synthesis, although the electrophysiological changes may also have been induced by factors other than translation dysfunction. Meanwhile, the experiments above were based on the exogenous expression of eCAGr RNA, and the contribution of endogenous eCAGr RNA to the disease is still unknown. Future studies of animal models expressing only the RNA are desired to address this question. In fact, aggregation-prone proteins have been discovered to be associated with neurodegeneration for decades, and yet the causal relationship and pathogenic mechanisms are still unclear for most neurodegenerative disorders. Meanwhile, the polyQ protein is most likely the dominant contributor to the disease, because the CAA·CAG models exhibit disease-relevant phenotypes[53], and enhancement of the polyQ protein degradation leads to significant rescue[54].

Discussion

RNA toxicity has been implicated in many repeat expansion diseases, and aberrant recruitment of RNA-binding proteins (RBPs) is thought to be one of the core mechanisms[55]. Repeat expansion RNAs may cause toxicity by over-recruiting certain RBPs to deplete them from the nucleoplasm. For example, in myotonic dystrophy, the alternative splicing factors, MBNL proteins, are sequestered by expanded CUG repeat RNA in the nucleus[56]. This leads to

transcriptome-wide spliceopathy that may cause the disease[57]. In addition to their functions in the nucleus, RBPs have important roles in the cytoplasm, and the sequestration of RBPs in the nucleus by repeat expansion RNAs can shift them away from the cytoplasm to compensate for reduced nuclear activity, thereby exacerbating the effects of RNA toxicity[58]. We tested U2af65, a known eCAGr RNA binding protein[59], and observe that it is also present in the cytoplasmic eCAGr RNA foci upon NH_4Cl treatment (Extended Data Fig. 9c). Thus, RNautophagy may also contribute to the eCAGr RNA-mediated pathogenic events beyond the observation in this study via clearance of these proteins. RBPs may also play a role in the different lysosomal sensitivity of nuclear versus cytoplasmic RNA foci. The difference between cytoplasmic and nuclear RNA foci in terms of their proteinaceous content may influence their subcellular localization, interaction with Lamp2c, and recognition by the lysosomes.

It has been a long-standing enigma that RNA foci are mainly localized in the nucleus, although nuclear RNA foci are not correlated with neurodegeneration[17]. For instance, eCAGr RNA foci and C9orf72 RNA foci are largely enriched in the nucleus[1, 60, 61]. Our study may provide clues to resolve this mystery: the cytoplasmic eCAGr foci do exist and exhibit the solid-like property that is consistent with their *in vitro* behavior, but they are subject to rapid lysosomal clearance. This demonstrates the role of lysosomal degradation in the clearance of eCAGr RNA foci, providing new entry points for the intervention of eCAGr RNA repeat expansion disorders.

We revealed that the eCAGr RNA leads to defects in global protein synthesis (Fig. 3). Recently, the change of global protein synthesis rates in repeat expansion disorders such as HD has been studied but remained controversial, with both upregulation and downregulation of global translation rates reported in different studies[28-33]. The reported mechanisms have also been fundamentally different. Nuclear accumulation of C9orf72 GGGGCC repeat expansion represses

translation possibly *via* defective nuclear export of mRNAs[62]. It may also trigger the activation of integrated stress response (ISR) and eIF2a phosphorylation (p-eIF2a), causing p-eIF2a-dependent stress granule formation and translation suppression[63]. The p-eIF2a levels were also reported to be elevated in culture models of HD and patient samples[64], although we failed to detect this change in the HD striatal cell line that showed translation suppression (Extended Data Fig. 10a). Thus, the global protein synthesis in repeat expansion disorders is likely influenced by multiple mechanisms, and the ultimate outcome could be variable depending on the experimental models, conditions, and measurement approaches. The *in vivo* expression of the eCAGr RNA induced motor function deficits and reduced synaptic strength (Fig. 8), possibly due to suppressed protein synthesis, which is known to play a key role in synaptic transmission[65, 66]. Meanwhile, the AAV expression mouse model has limitations and the pathogenic contributions of endogenous mutant RNA in these diseases remain to be further validated, ideally in large animal genetic models[47].

Both soluble eCAGr RNA and its gelation may contribute to the suppression of global protein synthesis. We observed strong colocalization between eEF2 puncta and eCAGr RNA foci (Fig. 7 and Extended Data Fig. 7a), suggesting that the RNA gels do trap eEF2, which is likely a major contributor to translation suppression. We speculate that the eEF2 is trapped during the RNA foci formation through its interaction with soluble eCAGr RNA. Meanwhile, the pre-formed solid-like RNA foci in absence of eEF2 may not be able to sequester eEF2 later and thus may not influence protein synthesis. This was confirmed by the *in vitro* phase-separation and translation experiments (Extended Data Fig. 10b-c). The observation that eCAGr RNA expression inhibited global protein synthesis both in the presence and the absence of lysosome inhibitors (Extended Data Fig.2e) is consistent with the involvement of RNA gelation. In both cases, these foci sequester eEF2 during their formation in a similar way, resulting in suppression of global protein translation

(Fig. 7e), whereas the lysosomal blockade by inhibitors or in aged animal/human tissues only enables us to better observe the eEF2 condensates (Fig. 6c; Extended Data Fig.5b & 7d). Taken together, the soluble eCAGr RNA may interact with eEF2, while RNA gelation in the presence of eEF2 likely sequester it to suppress protein synthesis. Meanwhile, the soluble eCAGr RNA may also play a role in protein synthesis suppression.

Our study suggests a novel mechanism of eEF2-mediated translation regulation: its sequestration by RNA gelation. Previous eEF2 studies mainly focused on its phosphorylation[45]. In contrast, cytoplasmic eCAGr RNA impaired the global translation *via* the recruitment of eEF2 into solid-like cytoplasmic RNA foci. This may have profound pathophysiological effects because deficient elongation causes not only a lower translational output but also potentially compromised translation fidelity. An eEF2 mutation in SCA26 causes a reduced translational fidelity and increased susceptibility to proteostatic insult[67]. Disturbances in eEF2-dependent ribosome translocation along the mRNA may influence various neuronal functions both outside of aging and in neurodegenerative diseases (reviewed in[68]). Besides eEF2, cytoplasmic eCAGr RNA foci likely contain many other proteins, similar to other cytoplasmic condensates such as stress granules. eEF2 may provide useful clues to identify these proteins, which may play additional roles in eCAGr RNA-related physiology or pathophysiology functions.

In summary, our discoveries revealed the novel cytoplasmic RNA gelation and its suppression of global protein translation elongation *via* eEF2 sequestration. The contribution of eCAGr RNA gelation toxicity in neurodegeneration remains to be studied. Interestingly, the rate of protein elongation was estimated to decline up to 80% during ageing[69]. Consistent with this, up to a 2-fold decrease in elongation rate in aged rat tissues relative to young counterparts was reported[70, 71]. The decreased protein translation could be a compensatory mechanism to prevent

cell death during ageing[72], but this might be exacerbated in CAG repeat expansion disorders, leading to loss of critical neuronal functions or neurodegeneration. The potential synergic effects between ageing and eCAGr RNA-induced lowering of global protein translation remain to be further explored.

References

1. Jain, A. & Vale, R.D. RNA phase transitions in repeat expansion disorders. *Nature* **546**, 243-247 (2017).
2. La Spada, A.R. & Taylor, J.P. Repeat expansion disease: progress and puzzles in disease pathogenesis. *Nat Rev Genet* **11**, 247-258 (2010).
3. Gardiner, S.L. *et al.* Prevalence of Carriers of Intermediate and Pathological Polyglutamine Disease-Associated Alleles Among Large Population-Based Cohorts. *JAMA Neurol* **76**, 650-656 (2019).
4. Consortium, G.M.o.H.s.D. CAG Repeat Not Polyglutamine Length Determines Timing of Huntington's Disease Onset. *Cell* **178**, 887-900 e814 (2019).
5. Banez-Coronel, M. *et al.* RAN Translation in Huntington Disease. *Neuron* **88**, 667-677 (2015).
6. Jazurek-Ciesiolka, M. *et al.* RAN Translation of the Expanded CAG Repeats in the SCA3 Disease Context. *J Mol Biol* **432**, 166699 (2020).
7. Zu, T. *et al.* Non-ATG-initiated translation directed by microsatellite expansions. *Proc Natl Acad Sci U S A* **108**, 260-265 (2011).
8. Yang, S. *et al.* Lack of RAN-mediated toxicity in Huntington's disease knock-in mice. *Proc Natl Acad Sci U S A* **117**, 4411-4417 (2020).
9. Arteaga-Bracho, E.E. *et al.* Postnatal and adult consequences of loss of huntingtin during development: Implications for Huntington's disease. *Neurobiology of disease* **96**, 144-155 (2016).
10. Becanovic, K. *et al.* A SNP in the HTT promoter alters NF-kappaB binding and is a bidirectional genetic modifier of Huntington disease. *Nat Neurosci* **18**, 807-816 (2015).
11. Rodan, L.H. *et al.* A novel neurodevelopmental disorder associated with compound heterozygous variants in the huntingtin gene. *Eur J Hum Genet* **24**, 1833 (2016).
12. Marti, E. RNA toxicity induced by expanded CAG repeats in Huntington's disease. *Brain Pathol* **26**, 779-786 (2016).
13. Schilling, J. *et al.* Deregulated Splicing Is a Major Mechanism of RNA-Induced Toxicity in Huntington's Disease. *J Mol Biol* **431**, 1869-1877 (2019).
14. Fay, M.M., Anderson, P.J. & Ivanov, P. ALS/FTD-Associated C9ORF72 Repeat RNA Promotes Phase Transitions In Vitro and in Cells. *Cell reports* **21**, 3573-3584 (2017).
15. Sanders, D.W. & Brangwynne, C.P. Neurodegenerative disease: RNA repeats put a freeze on cells. *Nature* **546**, 215-216 (2017).
16. Van Treeck, B. & Parker, R. Emerging Roles for Intermolecular RNA-RNA Interactions in RNP Assemblies. *Cell* **174**, 791-802 (2018).

17. Swinnen, B., Robberecht, W. & Van Den Bosch, L. RNA toxicity in non-coding repeat expansion disorders. *EMBO J* **39**, e101112 (2020).
18. Lamark, T. & Johansen, T. Aggrephagy: selective disposal of protein aggregates by macroautophagy. *Int J Cell Biol* **2012**, 736905 (2012).
19. Fujiwara, Y., Wada, K. & Kabuta, T. Lysosomal degradation of intracellular nucleic acids-multiple autophagic pathways. *J Biochem* **161**, 145-154 (2017).
20. Fujiwara, Y. *et al.* Discovery of a novel type of autophagy targeting RNA. *Autophagy* **9**, 403-409 (2013).
21. Trettel, F. *et al.* Dominant phenotypes produced by the HD mutation in STHdh(Q111) striatal cells. *Hum Mol Genet* **9**, 2799-2809 (2000).
22. Buchan, J.R., Kolaitis, R.M., Taylor, J.P. & Parker, R. Eukaryotic stress granules are cleared by autophagy and Cdc48/VCP function. *Cell* **153**, 1461-1474 (2013).
23. Zhang, Y. *et al.* SEPA-1 mediates the specific recognition and degradation of P granule components by autophagy in C. elegans. *Cell* **136**, 308-321 (2009).
24. Zhao, Y., Tian, E. & Zhang, H. Selective autophagic degradation of maternally-loaded germline P granule components in somatic cells during C. elegans embryogenesis. *Autophagy* **5**, 717-719 (2009).
25. Mehrpour, M., Esclatine, A., Beau, I. & Codogno, P. Overview of macroautophagy regulation in mammalian cells. *Cell research* **20**, 748-762 (2010).
26. Hase, K. *et al.* Cytosolic domain of SIDT2 carries an arginine-rich motif that binds to RNA/DNA and is important for the direct transport of nucleic acids into lysosomes. *Autophagy* **16**, 1974-1988 (2020).
27. Boeynaems, S. *et al.* Spontaneous driving forces give rise to protein-RNA condensates with coexisting phases and complex material properties. *Proc Natl Acad Sci U S A* **116**, 7889-7898 (2019).
28. Joag, H. *et al.* A role of cellular translation regulation associated with toxic Huntingtin protein. *Cell Mol Life Sci* **77**, 3657-3670 (2020).
29. Athar, Y.M. & Joseph, S. The Human Fragile X Mental Retardation Protein Inhibits the Elongation Step of Translation through Its RGG and C-Terminal Domains. *Biochemistry* **59**, 3813-3822 (2020).
30. Creus-Muncunill, J. *et al.* Increased translation as a novel pathogenic mechanism in Huntington's disease. *Brain* **142**, 3158-3175 (2019).
31. Brouillet, E. & Merienne, K. What is gained or 'lost in translation' in Huntington's disease. *Brain* **142**, 2900-2902 (2019).
32. Jacquemont, S. *et al.* Protein synthesis levels are increased in a subset of individuals with fragile X syndrome. *Hum Mol Genet* **27**, 2039-2051 (2018).
33. Eshraghi, M. *et al.* Mutant Huntingtin stalls ribosomes and represses protein synthesis in a cellular model of Huntington disease. *Nat Commun* **12**, 1461 (2021).
34. McGuire, A.M., Matsuo, H. & Wagner, G. Internal and overall motions of the translation factor eIF4E: cap binding and insertion in a CHAPS detergent micelle. *J Biomol NMR* **12**, 73-88 (1998).
35. Shieh, S.Y. & Bonini, N.M. Genes and pathways affected by CAG-repeat RNA-based toxicity in Drosophila. *Hum Mol Genet* **20**, 4810-4821 (2011).
36. Zhang, Q. *et al.* A peptidylic inhibitor for neutralizing expanded CAG RNA-induced nucleolar stress in polyglutamine diseases. *RNA* **24**, 486-498 (2018).

37. Bugaj, L.J., Choksi, A.T., Mesuda, C.K., Kane, R.S. & Schaffer, D.V. Optogenetic protein clustering and signaling activation in mammalian cells. *Nat Methods* **10**, 249-252 (2013).
38. Mann, J.R. *et al.* RNA Binding Antagonizes Neurotoxic Phase Transitions of TDP-43. *Neuron* **102**, 321-338 e328 (2019).
39. Sinturel, F. *et al.* Diurnal Oscillations in Liver Mass and Cell Size Accompany Ribosome Assembly Cycles. *Cell* **169**, 651-663 e614 (2017).
40. Schmidt, E.K., Clavarino, G., Ceppi, M. & Pierre, P. SUnSET, a nonradioactive method to monitor protein synthesis. *Nat Methods* **6**, 275-277 (2009).
41. Deng, Z. *et al.* Myostatin inhibits eEF2K-eEF2 by regulating AMPK to suppress protein synthesis. *Biochem Biophys Res Commun* **494**, 278-284 (2017).
42. Arguello, R.J. *et al.* SunRiSE - measuring translation elongation at single-cell resolution by means of flow cytometry. *J Cell Sci* **131** (2018).
43. Darnell, J.C. *et al.* FMRP stalls ribosomal translocation on mRNAs linked to synaptic function and autism. *Cell* **146**, 247-261 (2011).
44. Dever, T.E., Dinman, J.D. & Green, R. Translation Elongation and Recoding in Eukaryotes. *Cold Spring Harb Perspect Biol* **10** (2018).
45. Carlberg, U., Nilsson, A. & Nygard, O. Functional properties of phosphorylated elongation factor 2. *Eur J Biochem* **191**, 639-645 (1990).
46. Monkemeyer, L. *et al.* Chaperone Function of Hgh1 in the Biogenesis of Eukaryotic Elongation Factor 2. *Molecular cell* **74**, 88-100 e109 (2019).
47. Yan, S. *et al.* A Huntingtin Knockin Pig Model Recapitulates Features of Selective Neurodegeneration in Huntington's Disease. *Cell* **173**, 989-1002 e1013 (2018).
48. Crook, Z.R. & Housman, D. Huntington's disease: can mice lead the way to treatment? *Neuron* **69**, 423-435 (2011).
49. Feng, X., Luo, S. & Lu, B. Conformation Polymorphism of Polyglutamine Proteins. *Trends in biochemical sciences* **43**, 424-435 (2018).
50. Ariano, M.A. *et al.* Striatal potassium channel dysfunction in Huntington's disease transgenic mice. *J Neurophysiol* **93**, 2565-2574 (2005).
51. Kolodziejczyk, K., Parsons, M.P., Southwell, A.L., Hayden, M.R. & Raymond, L.A. Striatal synaptic dysfunction and hippocampal plasticity deficits in the Hu97/18 mouse model of Huntington disease. *PLoS One* **9**, e94562 (2014).
52. Sharma, V. *et al.* eIF2alpha controls memory consolidation via excitatory and somatostatin neurons. *Nature* **586**, 412-416 (2020).
53. Gray, M. *et al.* Full-length human mutant huntingtin with a stable polyglutamine repeat can elicit progressive and selective neuropathogenesis in BACHD mice. *J Neurosci* **28**, 6182-6195 (2008).
54. Li, Z. *et al.* Allele-selective lowering of mutant HTT protein by HTT-LC3 linker compounds. *Nature* **575**, 203-209 (2019).
55. Malik, I., Kelley, C.P., Wang, E.T. & Todd, P.K. Author Correction: Molecular mechanisms underlying nucleotide repeat expansion disorders. *Nat Rev Mol Cell Biol* **22**, 644 (2021).
56. Miller, J.W. *et al.* Recruitment of human muscleblind proteins to (CUG)(n) expansions associated with myotonic dystrophy. *EMBO J* **19**, 4439-4448 (2000).
57. Wang, E.T. *et al.* Transcriptome alterations in myotonic dystrophy skeletal muscle and heart. *Hum Mol Genet* **28**, 1312-1321 (2019).

58. Konieczny, P., Stepniak-Konieczna, E. & Sobczak, K. MBNL expression in autoregulatory feedback loops. *RNA Biol* **15**, 1-8 (2018).
59. Tsoi, H., Lau, C.K., Lau, K.F. & Chan, H.Y. Perturbation of U2AF65/NXF1-mediated RNA nuclear export enhances RNA toxicity in polyQ diseases. *Hum Mol Genet* **20**, 3787-3797 (2011).
60. Cooper-Knock, J. *et al.* Antisense RNA foci in the motor neurons of C9ORF72-ALS patients are associated with TDP-43 proteinopathy. *Acta Neuropathol* **130**, 63-75 (2015).
61. Mizielinska, S. *et al.* C9orf72 frontotemporal lobar degeneration is characterised by frequent neuronal sense and antisense RNA foci. *Acta Neuropathol* **126**, 845-857 (2013).
62. Rossi, S. *et al.* Nuclear accumulation of mRNAs underlies G4C2-repeat-induced translational repression in a cellular model of C9orf72 ALS. *J Cell Sci* **128**, 1787-1799 (2015).
63. Green, K.M. *et al.* RAN translation at C9orf72-associated repeat expansions is selectively enhanced by the integrated stress response. *Nat Commun* **8**, 2005 (2017).
64. Leitman, J. *et al.* ER stress-induced eIF2-alpha phosphorylation underlies sensitivity of striatal neurons to pathogenic huntingtin. *PLoS One* **9**, e90803 (2014).
65. Kelleher, R.J., 3rd, Govindarajan, A. & Tonegawa, S. Translational regulatory mechanisms in persistent forms of synaptic plasticity. *Neuron* **44**, 59-73 (2004).
66. Klann, E. & Dever, T.E. Biochemical mechanisms for translational regulation in synaptic plasticity. *Nat Rev Neurosci* **5**, 931-942 (2004).
67. Hekman, K.E. *et al.* A conserved eEF2 coding variant in SCA26 leads to loss of translational fidelity and increased susceptibility to proteostatic insult. *Hum Mol Genet* **21**, 5472-5483 (2012).
68. Knight, J.R.P. *et al.* Control of translation elongation in health and disease. *Dis Model Mech* **13** (2020).
69. Rattan, S.I. Synthesis, modifications, and turnover of proteins during aging. *Experimental gerontology* **31**, 33-47 (1996).
70. Merry, B.J. & Holehan, A.M. Effect of age and restricted feeding on polypeptide chain assembly kinetics in liver protein synthesis in vivo. *Mech Ageing Dev* **58**, 139-150 (1991).
71. Khasigov, P.Z. & Nikolaev, A. Age-related changes in the rates of polypeptide chain elongation. *Biochem Int* **15**, 1171-1178 (1987).
72. Steffen, K.K. & Dillin, A. A Ribosomal Perspective on Proteostasis and Aging. *Cell Metab* **23**, 1004-1012 (2016).

Supplementary Materials:

Materials and Methods with Additional References

Extended Data Figures 1-10

Supplementary Figure 1-3

Video S1-S2

Source Figure 1 (unprocessed full gel blots)

Source Data Table 1 (the excel sheet showing all data for plots)

695

Main figures and legends:

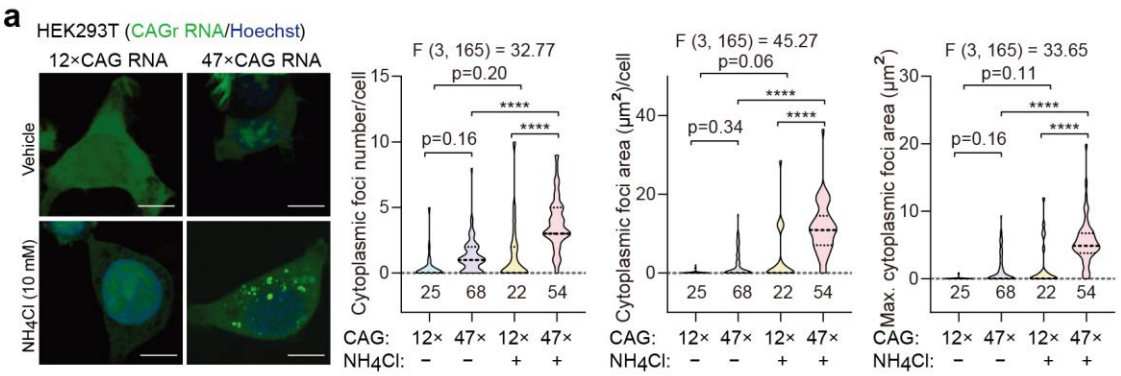

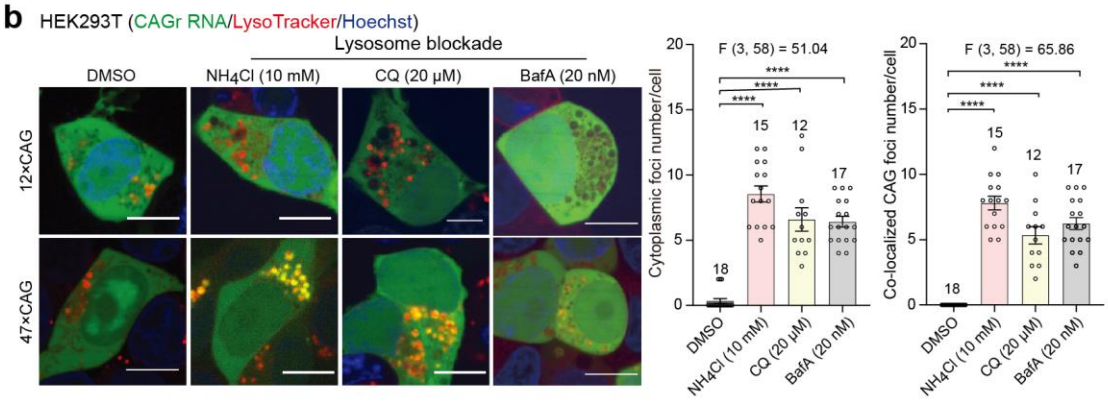

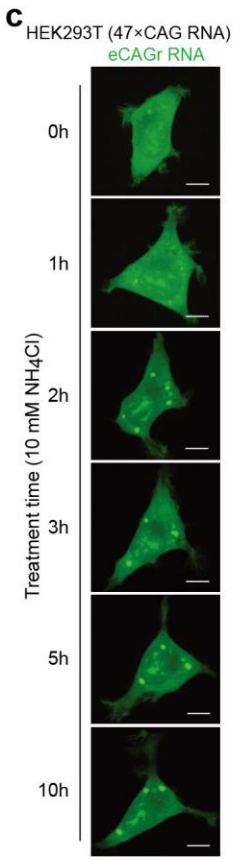

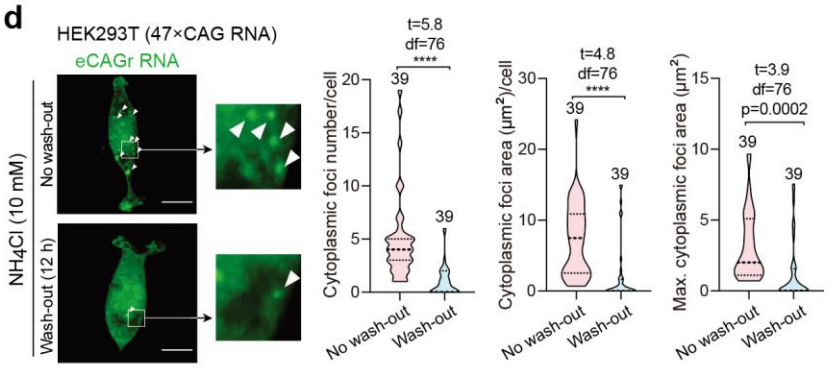

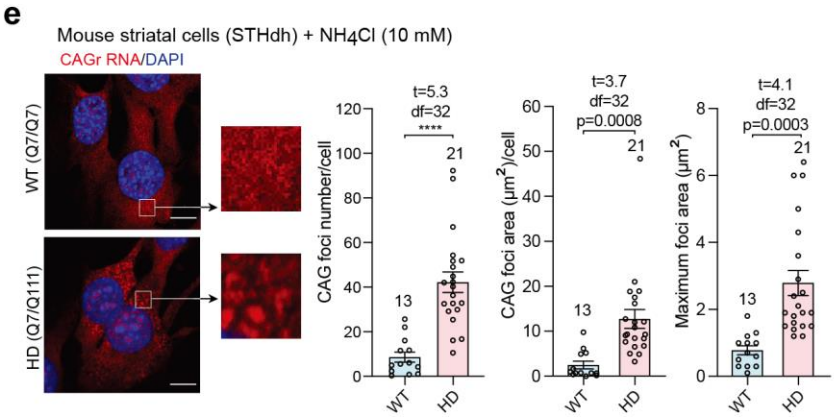

Fig. 1: The eCAGr RNA forms cytoplasmic gel-like condensates that are degraded by the lysosomes. a. Representative images and quantifications of eCAGr RNA condensates (foci) in transfected HEK293T cells expressing the indicated RNA together with MS2CP-YFP as the foci detector. **b.** Representative images and quantifications of eCAGr RNA foci and the lysosomes in HEK293T cells treated with the indicated lysosome inhibitors (NH_4Cl, chloroquine (CQ), or bafilomycin A1 (BafA)). **c-d.** Snap-shots and quantifications of the representative live-cell imaging (from 20) showing that the eCAGr RNA foci appeared in the cytoplasm after adding the lysosome inhibitor NH_4Cl but not the vehicle (culture medium) control (**c**), and disappeared after washing out NH_4Cl (**d**). eCAGr RNA foci are indicated by white arrows (**d**). **e**. Representative images and quantifications of RNA foci by RNA FISH in HD STHdh cells treated with the indicated lysosome inhibitors versus WT STHdh cells. Data are mean ± s.e.m.; analysed by one-way ANOVA with multiple comparisons (**a, b**), or unpaired two-tailed t tests (**d, e**). The numbers of cells are shown in each plot. ****: $p < 0.0001$. Scale bars, 10 μm (**a-e**).

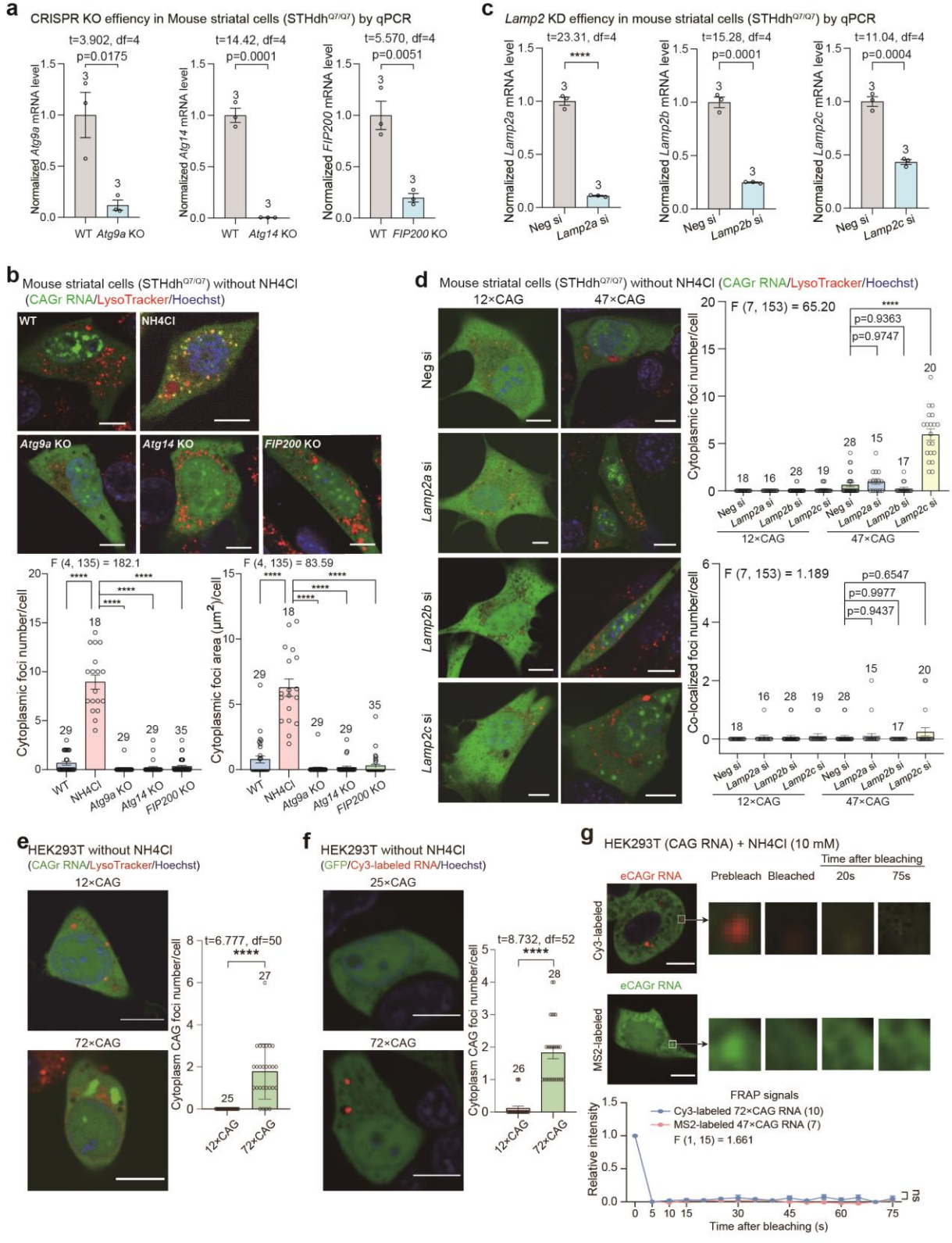
a
CRISPR KO effiency in Mouse striatal cells (STHdhQ7/Q7) by qPCR
t=3.902, df=4
p=0.0175
t=14.42, df=4
p=0.0001
t=5.570, df=4
p=0.0051
Normalized Atg9a mRNA level
Normalized Atg14 mRNA level
Normalized FIP200 mRNA level
WT Atg9a KO
WT Atg14 KO
WT FIP200 KO
c
Lamp2 KD effiency in mouse striatal cells (STHdhQ7/Q7) by qPCR
t=23.31, df=4
****
t=15.28, df=4
p=0.0001
t=11.04, df=4
p=0.0004
Normalized Lamp2a mRNA level
Normalized Lamp2b mRNA level
Normalized Lamp2c mRNA level
Neg si
Lamp2a si
Lamp2b si
Lamp2c si
b
Mouse striatal cells (STHdhQ7/Q7) without NH4Cl
(CAGr RNA/LysoTracker/Hoechst)
WT
NH4Cl
Atg9a KO
Atg14 KO
FIP200 KO
F (4, 135) = 182.1
F (4, 135) = 83.59
Cytoplasmic foci number/cell
Cytoplasmic foci area (μm2)/cell
d
Mouse striatal cells (STHdhQ7/Q7) without NH4Cl (CAGr RNA/LysoTracker/Hoechst)
12×CAG
47×CAG
Neg si
Lamp2a si
Lamp2b si
Lamp2c si
F (7, 153) = 65.20
p=0.9363
p=0.9747
Cytoplasmic foci number/cell
F (7, 153) = 1.189
p=0.6547
p=0.9977
p=0.9437
Co-localized foci number/cell
e
HEK293T without NH4Cl
(CAGr RNA/LysoTracker/Hoechst)
12×CAG
72×CAG
t=6.777, df=50
Cytoplasm CAG foci number/cell
f
HEK293T without NH4Cl
(GFP/Cy3-labeled RNA/Hoechst)
25×CAG
72×CAG
t=8.732, df=52
Cytoplasm CAG foci number/cell
g
HEK293T (CAG RNA) + NH4Cl (10 mM)
Time after bleaching
eCAGr RNA
Prebleach
Bleached
20s
75s
Cy3-labeled
MS2-labeled
FRAP signals
Cy3-labeled 72×CAG RNA (10)
MS2-labeled 47×CAG RNA (7)
F (1, 15) = 1.661
Relative intensity
Time after bleaching (s)
ns

Fig. 2. eCAGr RNA condensates were degraded by lysosomes *via* LAMP2C. a. qPCR experiments confirming the mRNA lowering in the indicated knock-out lines of STHdh cells generated by CRISPR/Cas9 (see supplementary Fig. 1 for DNA sequencing validation). **b.** Representative images and quantifications of cytoplasm eCAGr RNA foci (green, detected by MS2CP-YFP) in the indicated cell lines. While the lysosome inhibitor NH_4Cl treatment increased cytoplasmic foci, the knockout of key autophagy genes did not. **c.** qPCR experiments confirming the knockdown of the indicated mRNAs. **d.** Representative images and quantifications showing that cytoplasmic eCAGr RNA foci were formed outside the lysosomes in cells with *Lamp2c* knocked-down. **e**. Representative images and quantifications of eCAGr RNA condensates (foci) in transfected HEK293T cells expressing the indicated RNA with MS2CP-YFP as the foci detector but without NH_4Cl. **f**. Representative images and quantifications of Cy3-labeled eCAGr RNA condensates in HEK293T cells treated without NH_4Cl. **g.** Representative images and quantifications of the FRAP experiments for the eCAGr RNA foci in the cytoplasm using both the transfected Cy3-labeled eCAGr RNA (upper; GFP (green) co-transfected and Hoechst (blue) co-stained to visualize the cell and nuclei) and MS2 system (lower; the nuclear region is evident without Hoechst staining).Data are mean ± s.e.m.; analysed by two-tailed unpaired t tests (**a & c, e & f**) or one-way ANOVA with multiple comparisons (**b & d**) or two-way ANOVA(g). n indicates independently repeated wells (**a & c**) or the number of cells (**b, d & e-g**). Scale bars, 10 μm (**b, d & e-g**).

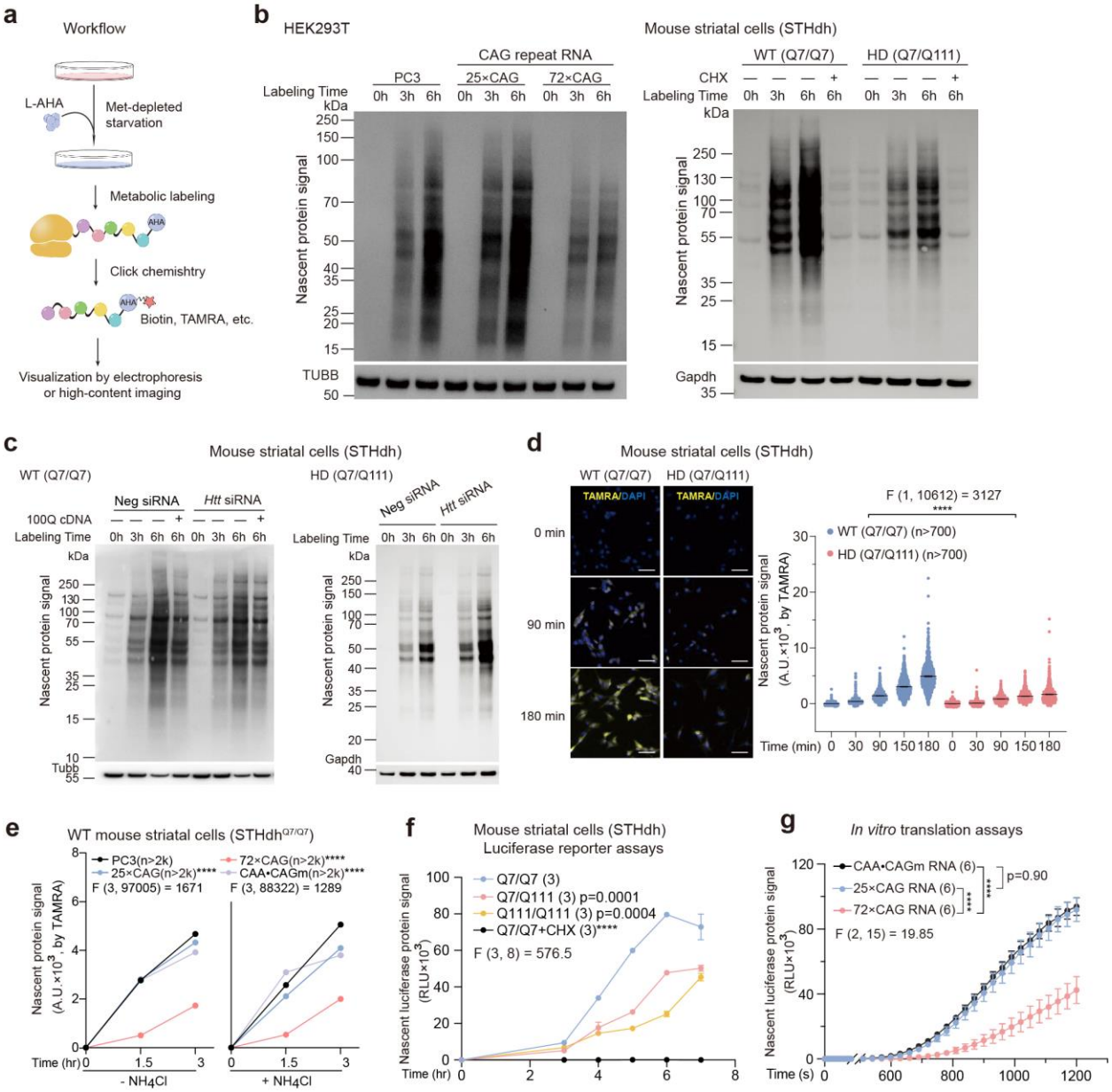

Fig. 3: The eCAGr RNA gelation inhibits global protein translation. a. Schematic showing the metabolic nascent protein labeling assays with the methionine analog L-AHA. **b.** Representative western-blots of nascent proteins at indicated time points after metabolic labeling in HEK293T transfected with the indicated plasmids for 24 hours (*left*) or HD mouse striatal cells ($STHdh^{Q7/Q111}$) expressing endogenous mutant *HTT* mRNA containing eCAGr, versus the WT cells ($STHdh^{Q7/Q7}$) expressing no eCAGr RNA (*right*). The nascent proteins were labeled for different lengths of time by the methionine analog L-AHA, which was then conjugated with biotin by Click-chemistry for detection using streptavidin-HRP. The protein translation inhibitor cycloheximide (CHX)-treated groups were tested in the STHdh cells to ensure the specificity of

the signals. **c.** Similar to a, but in STHdh cells transfected with the indicated siRNA or cDNA (100Q: full-length *HTT* cDNA containing 100×CAG). **d.** Representative high-content imaging and quantifications of nascent proteins in the $STHdh^{Q7/Q111}$ versus $STHdh^{Q7/Q7}$ cells at indicated time points after metabolic labeling. The nascent proteins were labeled for different lengths of time by the methionine analog L-AHA, which was then conjugated with TAMRA by Click-chemistry for visualization at the single-cell level after fixing the cells. **e.** Quantifications of high-content images of nascent proteins in $STHdh^{Q7/Q7}$ cells transfected with the indicated plasmids at indicated time points after metabolic labeling. The cells were treated with or without the lysosomal inhibitor NH_4Cl. **f.** The luciferase reporter assay measuring the protein translation rate in WT ($STHdh^{Q7/Q7}$) or HD ($STHdh^{Q7/Q111}$ and $STHdh^{Q111/Q111}$) mouse striatal cells upon transfection of the reporter mRNA. **g.** The luciferase reporter assay measuring the protein translation rate in the *in vitro* translation system (using rabbit reticulocyte cell extracts pretreated with the indicated RNAs for 5 minutes). Data are mean ± s.e.m.; analysed by two-way ANOVA with multiple comparisons (**d-g**). The numbers of cells (**d-e**) or the numbers of independently repeated wells (**f-g**) are shown in each plot. ****: $p < 0.0001$. Scale bars, 20 μm (**d**). Representative western-blots were all from ≥ 3 biological repeats; see Extended Data Fig. 2 for quantifications.

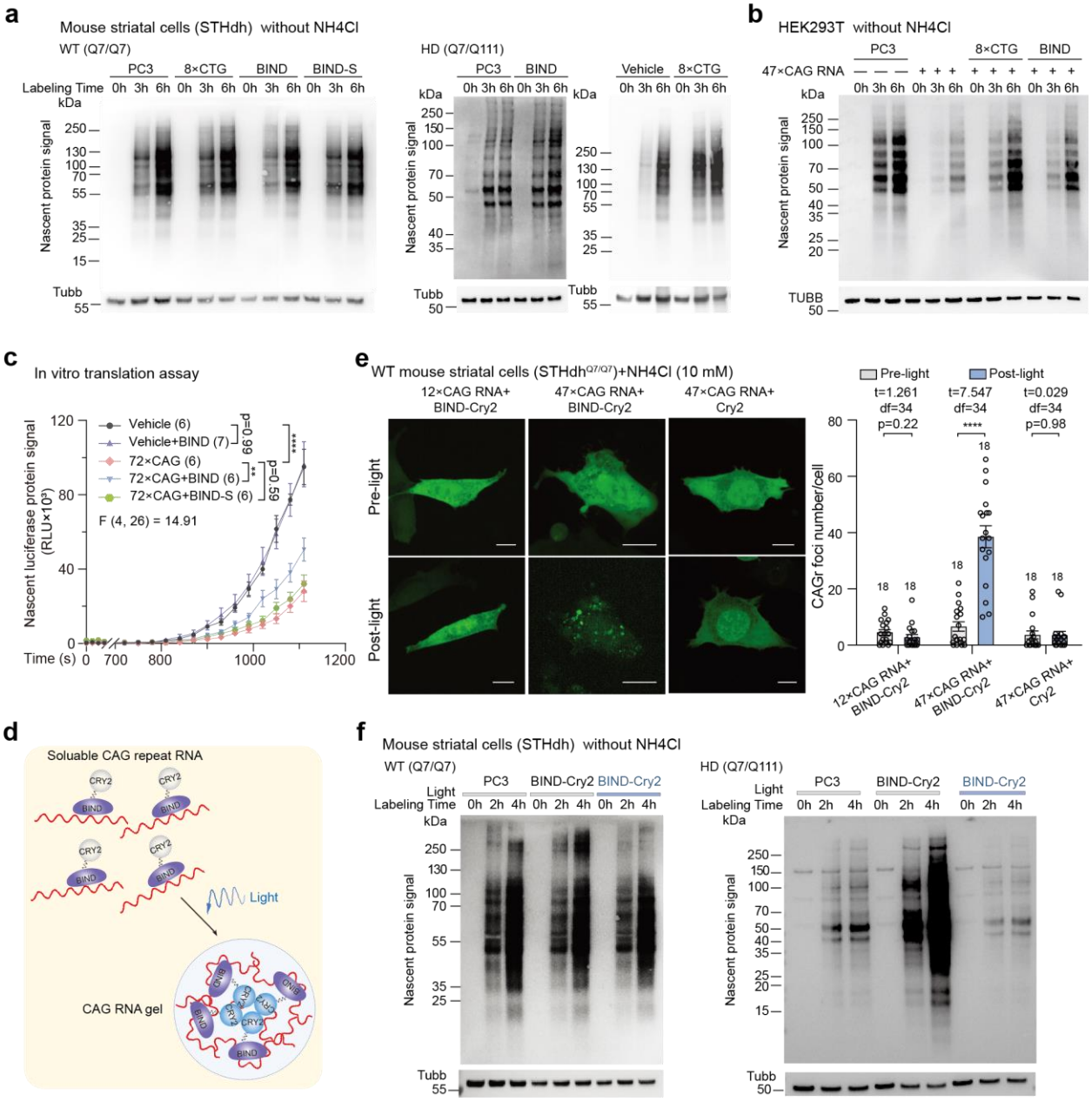

760 **Fig. 4: The RNA gelation is likely the major cause of global protein translation inhibition.**

a. Representative western-blots (from ⩾3) of nascent proteins at indicated time points after metabolic labeling in WT (Q7/Q7) or HD (Q7/Q111) mouse striatal cells transfected with the indicated oligonucleotides (8×CTG) or plasmids (empty pcDNA 3.0 vector (PC3) or the one expressing eCAGr RNA-binding peptide (BIND) versus the control (BIND-S)). **b.** Similar to a, 765 but in HEK293T cells. **c.** Luciferase reporter assay measuring the protein translation rate of the *in*

vitro translation system pre-treated with the indicated synthetic peptides and/or *in vitro* transcribed RNAs for 5 minutes. **d.** Schematic showing the optogenetic system that manipulates eCAGr RNA gelation: the blue light is used to trigger or enhance the assembly of eCAGr RNA condensates. **e.** Representative images and quantifications showing the enhanced clustering of eCAGr RNA upon the blue light stimulation in NH_4Cl-treated WT cells ($STHdh^{Q7/Q7}$) transfected with the indicated plasmids. **f.** Similar to **a**, but in WT or HD mouse striatal cells transfected with the indicated plasmids with (blue bars on top of the gel) or without (white bars on top of the gel) the blue light exposure. Enhancement in eCAGr RNA condensate formation disabled the rescue effect of BIND on protein translation which was suppressed by the eCAGr RNA gelation. Data are mean ± s.e.m.; analysed by two-way ANOVA with multiple comparisons (**c**) or two-tailed unpaired t tests (**e**). The numbers of independently repeated wells (**c**) or the numbers of cells (**e**) are shown in each plot. ****: $p < 0.0001$. Scale bars, 10 μm (**e**). Representative western-blots were all from $\geqslant 3$ biological repeats; see Extended Data Fig. 3 for quantifications.

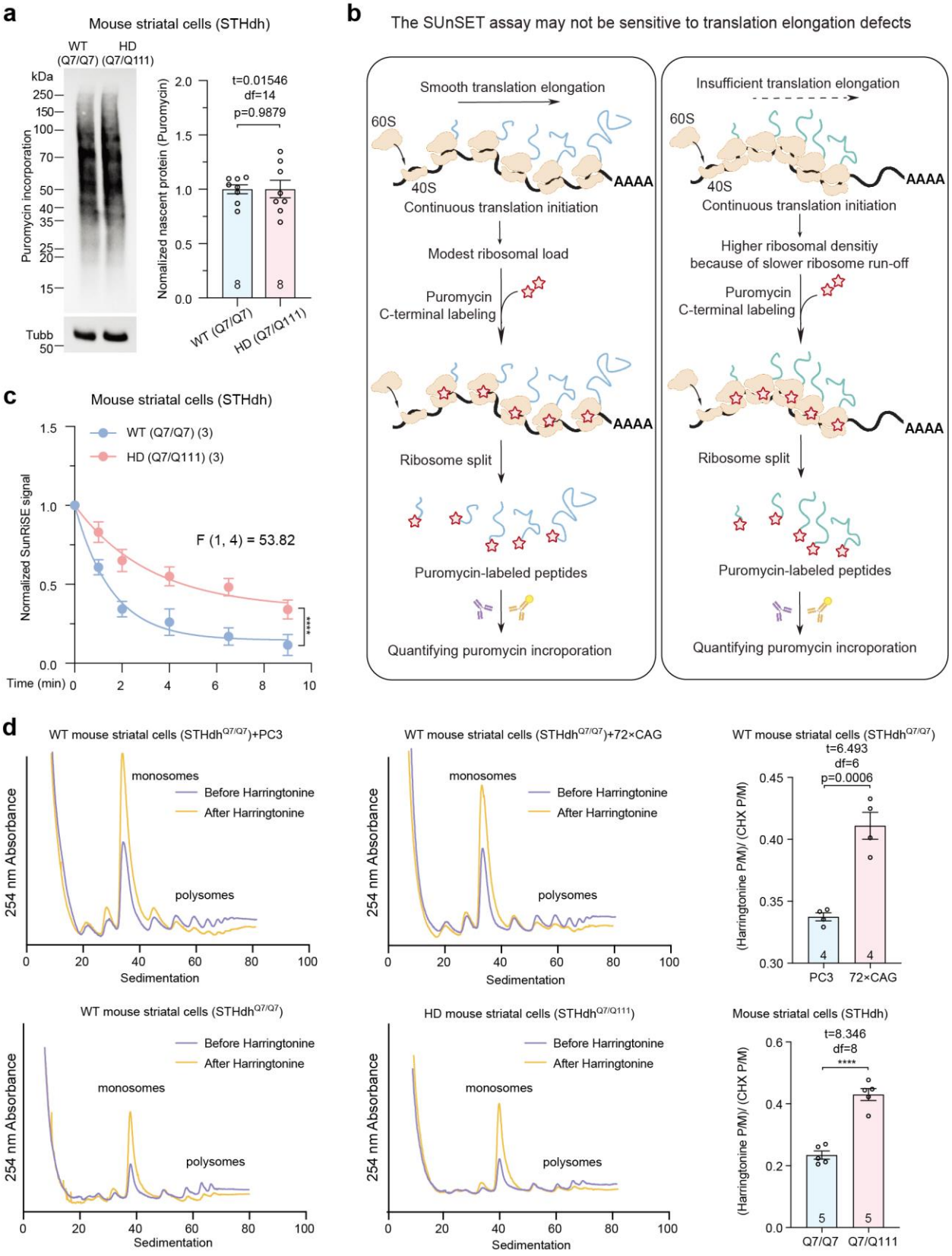
a
Mouse striatal cells (STHdh)
WT (Q7/Q7)
HD (Q7/Q111)
kDa
250
150
100
70
50
40
35
25
20
15
Puromycin incorporation
Tubb
50
Nomalized nascent protein (Puromycin)
2.0
1.5
1.0
0.5
0.0
t=0.01546
df=14
p=0.9879
8
8
WT (Q7/Q7)
HD (Q7/Q111)
b
The SUnSET assay may not be sensitive to translation elongation defects
Smooth translation elongation
60S
40S
AAAA
Continuous translation initiation
Modest ribosomal load
Puromycin
C-terminal labeling
Ribosome split
Puromycin-labeled peptides
Quantifying puromycin incroporation
Insufficient translation elongation
60S
40S
AAAA
Continuous translation initiation
Higher ribosomal densitiy
because of slower ribosome run-off
Puromycin
C-terminal labeling
Ribosome split
Puromycin-labeled peptides
Quantifying puromycin incroporation
c
Mouse striatal cells (STHdh)
WT (Q7/Q7) (3)
HD (Q7/Q111) (3)
Normalized SunRiSE signal
1.5
1.0
0.5
0.0
F (1, 4) = 53.82
****
Time (min)
0
2
4
6
8
10
d
WT mouse striatal cells (STHdhQ7/Q7)+PC3
monosomes
Before Harringtonine
After Harringtonine
polysomes
254 nm Absorbance
0
20
40
60
80
100
Sedimentation
WT mouse striatal cells (STHdhQ7/Q7)+72×CAG
monosomes
Before Harringtonine
After Harringtonine
polysomes
254 nm Absorbance
0
20
40
60
80
100
Sedimentation
WT mouse striatal cells (STHdhQ7/Q7)
t=6.493
df=6
p=0.0006
(Harringtonine P/M)/ (CHX P/M)
0.45
0.40
0.35
0.30
4
4
PC3
72×CAG
WT mouse striatal cells (STHdhQ7/Q7)
Before Harringtonine
After Harringtonine
monosomes
polysomes
254 nm Absorbance
0
20
40
60
80
100
Sedimentation
HD mouse striatal cells (STHdhQ7/Q111)
Before Harringtonine
After Harringtonine
monosomes
polysomes
254 nm Absorbance
0
20
40
60
80
100
Sedimentation
Mouse striatal cells (STHdh)
t=8.346
df=8
****
(Harringtonine P/M)/ (CHX P/M)
0.6
0.4
0.2
0.0
5
5
Q7/Q7
Q7/Q111

780

Fig. 5: The eCAGr RNA impairs the protein translation elongation. a. Representative gel images and quantifications of puromycin-labeled proteins in WT and HD mouse striatal cells in SUnSET assays. **b.** Schematic showing that the conventional SUnSET assay may not be able to reveal translation elongation defects. **c.** The plot of SunRiSE assay signals (detected by high-content imaging) showing a decrease of translation elongation in WT versus HD mouse striatal cells. **d.** Representative polysome profiles and quantifications of WT/HD mouse striatal cells or the transfected WT mouse striatal cells expressing 72×CAG RNA, before versus after ribosome run-off. The polysome-to-monosome (P/M) ratio was calculated for each plot, and ratio between the P/M after 3 min harringtonine treatment (Harringtonine P/M) and the P/M before harringtonine treatment (CHX P/M, treated with cycloheximide alone without pre-treatment of harringtonine for 3 min) was quantified for the run-off rate. Data are mean ± s.e.m.; analysed by two-tailed unpaired t test (**a**, **d**) or two-way ANOVA (**c**). The numbers of independently repeated assays (**a**, **c**, **& d**) are shown in each plot. ****: $p < 0.0001$.

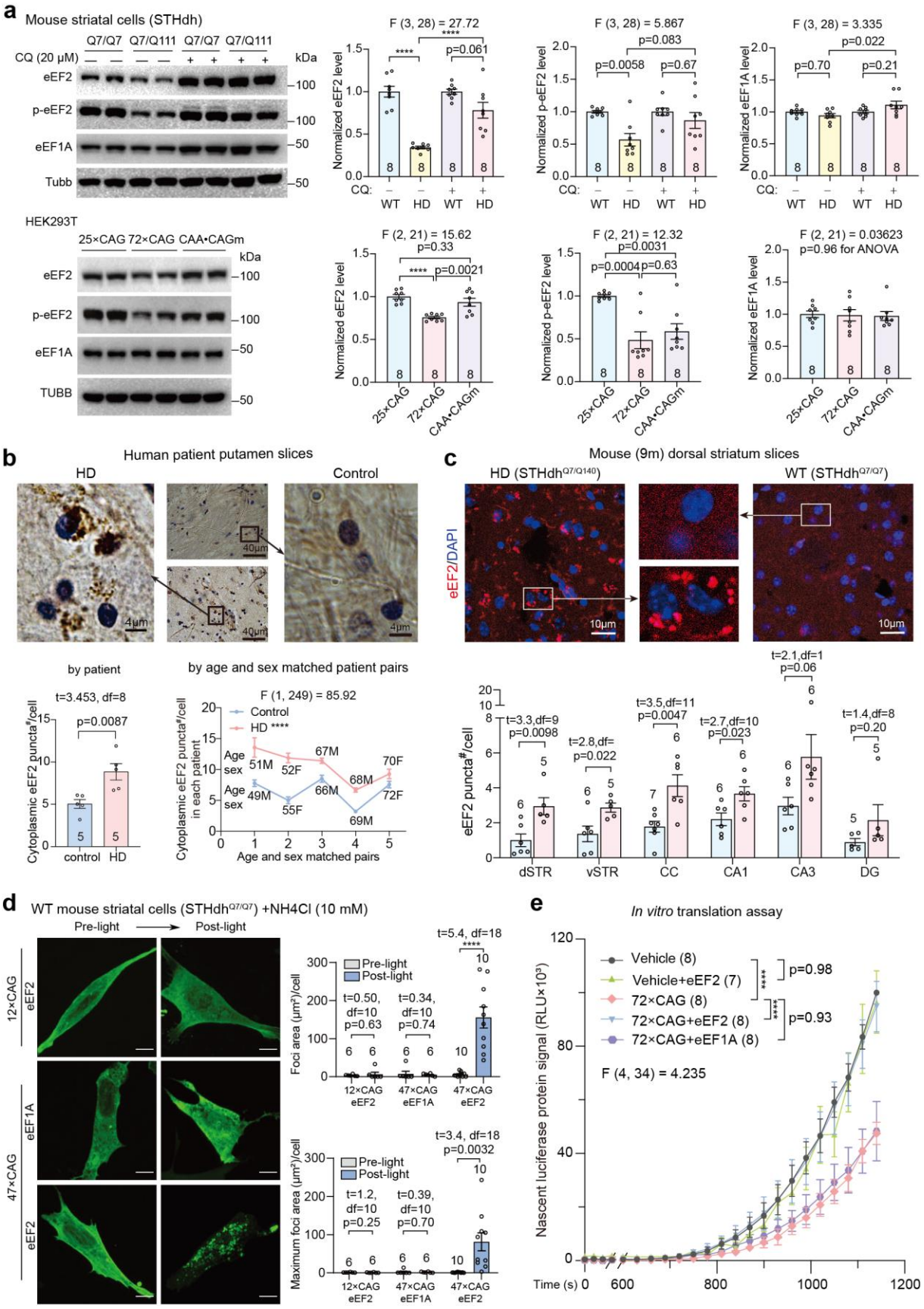
a
Mouse striatal cells (STHdh)
Q7/Q7 Q7/Q111 Q7/Q7 Q7/Q111
CQ (20 μM)
kDa
eEF2
p-eEF2
eEF1A
Tubb
HEK293T
25×CAG 72×CAG CAA•CAGm
TUBB
F (3, 28) = 27.72
F (3, 28) = 5.867
F (3, 28) = 3.335
F (2, 21) = 15.62
p=0.33
F (2, 21) = 12.32
F (2, 21) = 0.03623
p=0.96 for ANOVA
Normalized eEF2 level
Normalized p-eEF2 level
Normalized eEF1A level
WT HD WT HD
25×CAG 72×CAG CAA•CAGm
b
Human patient putamen slices
HD
Control
by patient
by age and sex matched patient pairs
Cytoplasmic eEF2 puncta#/cell
t=3.453, df=8
p=0.0087
control HD
F (1, 249) = 85.92
Control
HD ****
Age sex
Age and sex matched pairs
c
Mouse (9m) dorsal striatum slices
HD (STHdhQ7/Q140)
WT (STHdhQ7/Q7)
eEF2/DAPI
eEF2 puncta#/cell
dSTR vSTR CC CA1 CA3 DG
d
WT mouse striatal cells (STHdhQ7/Q7) +NH4Cl (10 mM)
Pre-light
Post-light
12×CAG eEF2
47×CAG eEF1A
47×CAG eEF2
Foci area (μm²)/cell
Maximum foci area (μm²)/cell
t=5.4, df=18
t=3.4, df=18
p=0.0032
e
In vitro translation assay
Vehicle (8)
Vehicle+eEF2 (7)
72×CAG (8)
72×CAG+eEF2 (8)
72×CAG+eEF1A (8)
p=0.98
p=0.93
F (4, 34) = 4.235
Nascent luciferase protein signal (RLU×10³)
Time (s)

Fig. 6: eCAGr RNA foci induces eEF2 clustering and degradation. a. Representative western-blots and quantifications of eEF2, phospho-eEF2, and eEF1A levels in the indicated cells treated/transfected with the indicated compounds or plasmids, respectively. CQ: chloroquine. **b.** Representative immunohistochemistry images (from > 25 images per patient) and quantifications (in total or within the age-matched pairs) showing the endogenous cytoplasmic eEF2 puncta in HD versus WT human putamen slices. **c.** Representative immunofluorescence images of dorsal striatum and quantifications of diverse brain sections showing the eEF2 puncta in HD ($Hdh^{Q7/Q140}$) versus WT ($Hdh^{Q7/Q7}$) mouse slices (n indicates the number of mice). **d.** Snapshots of representative live-cell imaging and quantifications of exogenously expressed eEF2-sfGFP or eEF1A-sfGFP puncta in NH_4Cl-treated WT or HD mouse striatal cells upon blue light exposure. Scale bars: 10 μm. **e.** Luciferase reporter assay measuring the translation rate in the *in vitro* translation system pre-treated with the indicated recombinant purified proteins and/or *in vitro* transcribed RNAs for 5 minutes. Data are mean ± s.e.m.; analysed by one-way ANOVA with multiple comparisons (**a**), two-way ANOVA (**b),** two-way ANOVA with multiple comparisons (**e**), or two-tailed unpaired t tests (**b**-**d**). The numbers of independently repeated samples (**a**), images **(b)**, mice (**c**), wells (**e**), or the numbers of cells (**d**) are shown in each plot. ****: $p < 0.0001$.

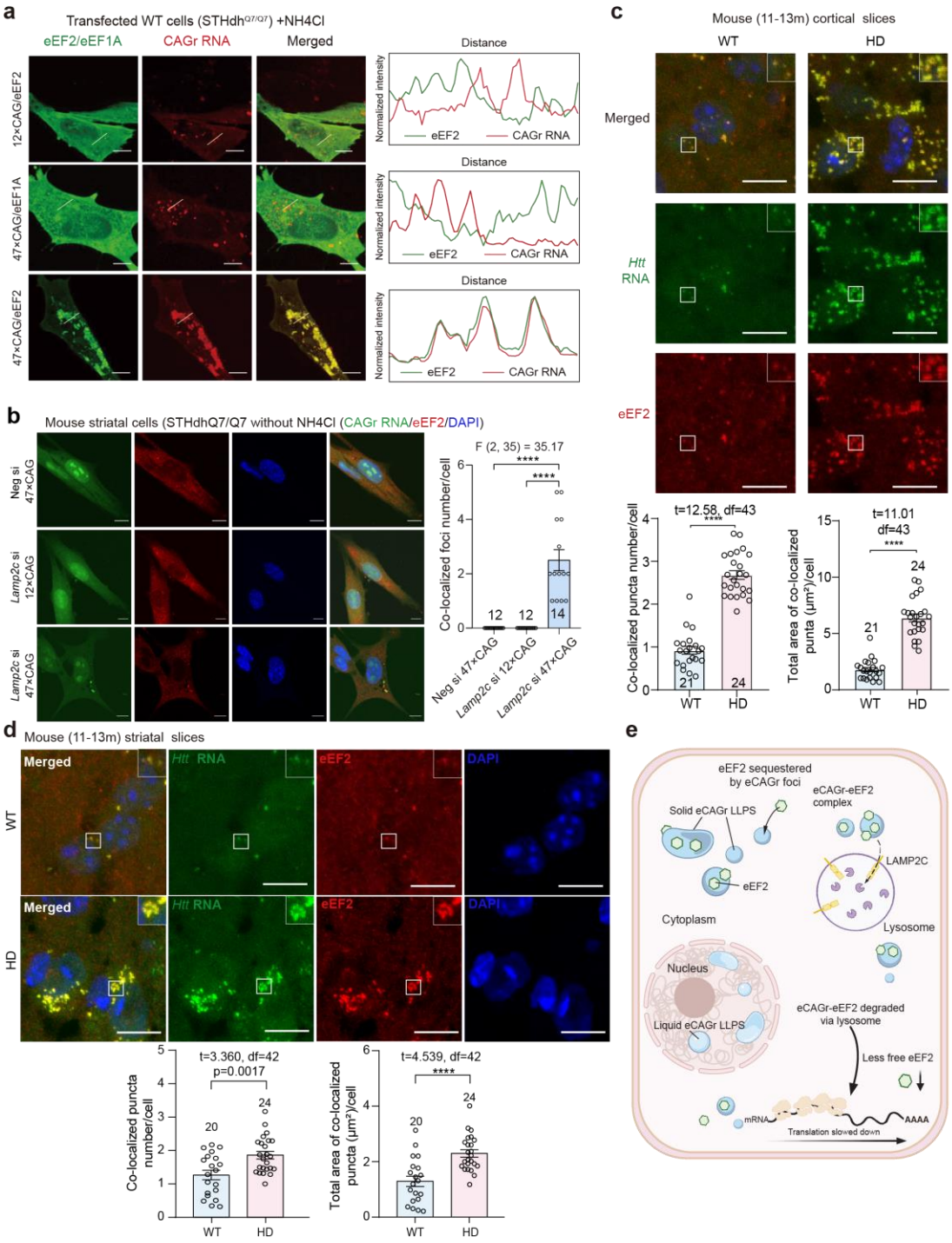

Fig. 7: eCAGr RNA foci sequester eEF2. a. Representative fluorescence images (from > 6) of
815 NH_4Cl-treated WT mouse striatal cells co-transfected with eCAGr RNA (47×CAG-MS2),

MS2CP-BFP, eEF2-sfGFP or eEF1A-sfGFP. The 12×CAG-MS2, MS2CP-BFP, and eEF2-sfGFP were also transfected into the cells for the control purpose. Colocalization patterns between eCAGr RNA and eEF2/eEF1A at the beige lines are plotted. **b**. Representative images and quantifications showing that cytoplasmic eCAGr RNA foci were co-localized with eEF2 puncta in cells with *Lamp2c* knocked-down.**c-d.** Representative images and quantifications showing the colocalization between endogenous eCAGr RNA foci (detected by RNA FISH) and eEF2 puncta (detected by immunofluorescence with the antibody validated in Extended Data Fig. 7d) in cortical (**c**) and striatal slices (**d**) from the HD versus WT mice. **e.** Schematic showing that the eCAGr RNA foci sequesters eEF2 and are subject to lysosomal clearance *via* LAMP2C, leading to global protein translation deficits. Data are mean ± s.e.m.; analysed by one-way ANOVA with multiple comparisons (**b**) or two-tailed unpaired t tests (**c & d**). ****: $p < 0.0001$. n indicates the number of cells (b) or the number of slices from 3 mice (**c & d**). Scale bars, 10 μm.

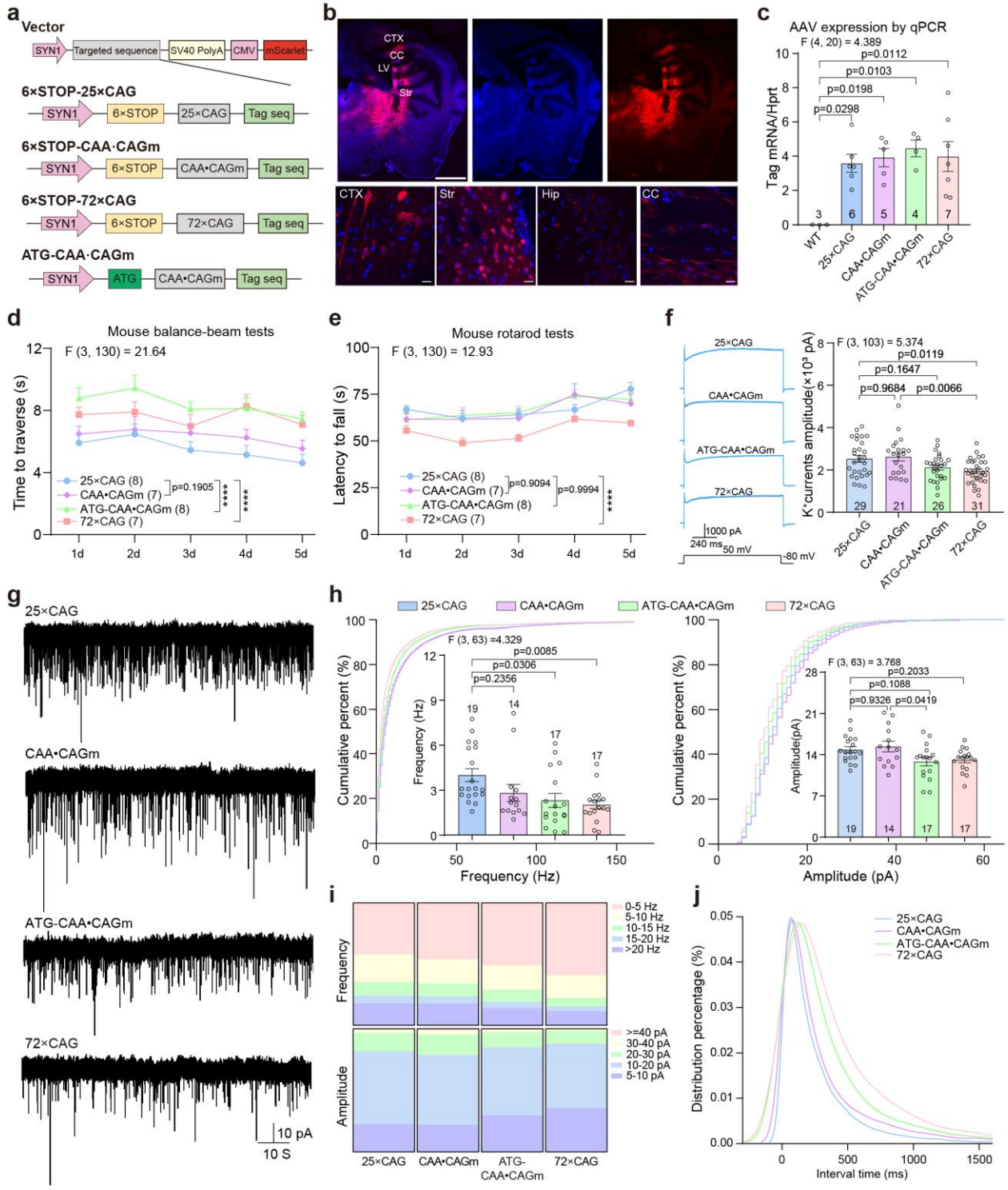
a
Vector
SYN1
Targeted sequence
SV40 PolyA
CMV
mScarlet
6×STOP-25×CAG
6×STOP
25×CAG
Tag seq
6×STOP-CAA·CAGm
CAA•CAGm
6×STOP-72×CAG
72×CAG
ATG-CAA·CAGm
ATG
b
CTX
CC
LV
Str
Hip
c
AAV expression by qPCR
F (4, 20) = 4.389
Tag mRNA/Hprt
p=0.0298
p=0.0198
p=0.0103
p=0.0112
WT
25×CAG
CAA•CAGm
ATG-CAA•CAGm
72×CAG
d
Mouse balance-beam tests
F (3, 130) = 21.64
Time to traverse (s)
25×CAG (8)
CAA•CAGm (7)
ATG-CAA•CAGm (8)
72×CAG (7)
p=0.1905
****
1d
2d
3d
4d
5d
e
Mouse rotarod tests
F (3, 130) = 12.93
Latency to fall (s)
p=0.9094
p=0.9994
f
25×CAG
CAA•CAGm
ATG-CAA•CAGm
72×CAG
1000 pA
240 ms
50 mV
-80 mV
F (3, 103) = 5.374
K+currents amplitude(×10³ pA)
p=0.0119
p=0.1647
p=0.9684
p=0.0066
g
25×CAG
CAA•CAGm
ATG-CAA•CAGm
72×CAG
10 pA
10 S
h
F (3, 63) =4.329
Cumulative percent (%)
Frequency (Hz)
p=0.0085
p=0.0306
p=0.2356
F (3, 63) = 3.768
Amplitude(pA)
p=0.2033
p=0.1088
p=0.9326
p=0.0419
Amplitude (pA)
i
Frequency
Amplitude
0-5 Hz
5-10 Hz
10-15 Hz
15-20 Hz
>20 Hz
>=40 pA
30-40 pA
20-30 pA
10-20 pA
5-10 pA
ATG-CAA•CAGm
j
Distribution percentage (%)
Interval time (ms)

830

Fig. 8: eCAGr RNA expression by AAV injection causes behavioural and electrophysiological phenotypes. a. Vector diagrams of 25×CAG, 72×CAG, CAA·CAGm, and ATG-CAA·CAGm co-expressed with the florescent protein mScarlet driven by an independent promoter (SYN1 and CMV, respectively) in bicistronic plasmids. **b.** Representative fluorescence images illustrating the AAV virus expression (red: mScarlet; blue: DAPI). Scale bars, 1mm (top) and 20 μm (bottom). CTX, cortex; CC, corpus callosum; LV, lateral ventricle; Str, striatum; Hip, hippocampus. **c.** RT-qPCR results illustrating AAV9-mediated expression of the indicated mRNAs in the striatum 5 weeks after injection. **d-e.** Quantifications of mouse behavioural performance in the balance beam (d) and rotarod (e) tests. **f.** Representative recordings and quantifications of the outward K^+ currents recorded from visually identified AAV-infected MSNs in striatal slices from indicated groups. **g-h.** Representative recordings and indicated quantifications of sEPSC recorded from visually identified AAV-infected MSNs in striatal slices from indicated groups. **i.** The category analyses showing that the proportion of low frequency (0-5Hz) and low amplitude (5-10pA) sEPSC events in the 72×CAG group. **j.** Distribution of the sEPSC event interval time in visually identified AAV-infected MSNs of the indicated groups. The expression of 72×CAG or ATG-CAA·CAGm led to a right shift of the peak in the distribution illustrating longer interval times. For all the electrophysiology recordings, the AAV-infected MSNs were visually picked in striatal slices and the action potentials were measured to confirm their neuronal identity. n indicates the number of mice (**c-e**) or the number of neurons from multiple mice (**f-h**). Statistical analysis was performed by one-way ANOVA with multiple comparisons (**c, f-h**) or two-way ANOVA with multiple comparisons (**d-e**).